Atlantic Thermohaline Circulation in a Coupled General Circulation Model: Unforced Variations versus Forced Changes

AIGUO DAI, A. HU, G. A. MEEHL, W. M. WASHINGTON, AND W. G. STRAND

National Center for Atmospheric Research, Boulder, Colorado*

(Manuscript received 30 September 2004, in final form 10 March 2005)

ABSTRACT

A 1200-yr unforced control run and future climate change simulations using the Parallel Climate Model (PCM), a coupled atmosphere–ocean–land–sea ice global model with no flux adjustments and relatively high resolution (~2.8° for the atmosphere and 2/3° for the oceans) are analyzed for changes in Atlantic Ocean circulations. For the forced simulations, historical greenhouse gas and sulfate forcing of the twentieth century and projected forcing for the next two centuries are used. The Atlantic thermohaline circulation (THC) shows large multidecadal (15–40 yr) variations with mean-peak amplitudes of 1.5–3.0 Sv (1 Sv $\equiv 10^6$ m^3 s^{-1}) and a sharp peak of power around a 24-yr period in the control run. Associated with the THC oscillations, there are large variations in North Atlantic Ocean heat transport, sea surface temperature (SST) and salinity (SSS), sea ice fraction, and net surface water and energy fluxes, which all lag the variations in THC strength by 2–3 yr. However, the net effect of the SST and SSS variations on upper-ocean density in the midlatitude North Atlantic leads the THC variations by about 6 yr, which results in the 24-yr period. The simulated SST and sea ice spatial patterns associated with the THC oscillations resemble those in observed SST and sea ice concentrations that are associated with the North Atlantic Oscillation (NAO). The results suggest a dominant role of the advective mechanism and strong coupling between the THC and the NAO, whose index also shows a sharp peak around the 24-yr time scale in the control run. In the forced simulations, the THC weakens by ~12% in the twenty-first century and continues to weaken by an additional ~10% in the twenty-second century if CO_2 keeps rising, but the THC stabilizes if CO_2 levels off. The THC weakening results from stabilizing temperature increases that are larger in the upper and northern Atlantic Ocean than in the deep and southern parts of the basin. In both the control and forced simulations, as the THC gains (loses) strength and depth, the separated Gulf Stream (GS) moves southward (northward) while the subpolar gyre centered at the Labrador Sea contracts from (expands to) the east with the North Atlantic Current (NAC) being shifted westward (eastward). These horizontal circulation changes, which are dynamically linked to the THC changes, induce large temperature and salinity variations around the GS and NAC paths.

1. Introduction

Atlantic Ocean circulations, in particular the thermohaline circulation (THC), have large impacts on regional and global climate (Rahmstorf 2002). Because of this, the natural variability of the THC and its potential response to anthropogenic forcing have attracted considerable attention (e.g., Broecker 1987, 1997; Rahmstorf 1999). Paleoceanographic records suggest that the THC exhibited different modes during the last glacial cycle and its mode changes have been linked to abrupt climate changes over the North Atlantic region (Clark et al. 2002). Early ocean model studies suggest that the THC may have multiple equilibrium states (Stommel 1961; Bryan 1986). More recent studies show that the THC may exhibit a hysteresis behavior in which it can have two distinct states for a given value of the control variable (e.g., heat or freshwater flux; Stocker and Wright 1991; Mikolajewicz and Maier-Reimer 1994; Rahmstorf 1995), which is a common feature of nonlinear physical systems. A number of model studies on low-frequency THC variability have focused on the relative role of thermal and haline forcing in driving the variation (e.g., Marotzke and Willebrand 1991; Weaver

* The National Center for Atmospheric Research is sponsored by the National Science Foundation.

Corresponding author address: Aiguo Dai, NCAR, P.O. Box 3000, Boulder, CO 80307.
E-mail: adai@ucar.edu

and Sarachik 1991; Delworth et al. 1993; Weaver et al. 1993; Winton and Sarachik 1993; Lenderink and Haarsma 1994), but often with divergent results.

There are two principal feedback mechanisms that cause changes in Atlantic THC: advective and convective feedbacks (Weaver and Sarachik 1991; Rahmstorf et al. 1996; Stocker 2000). In the Atlantic, wind-driven ocean circulation advects warm and salty subtropical water into the mid- and high latitudes. If this supply of salt and heat into the Atlantic sinking regions is perturbed due to changes in oceanic volume transport and/or large-scale surface heat and freshwater fluxes [e.g., those associated with the North Atlantic Oscillation (NAO)], then the formation rate of North Atlantic Deep Water (NADW) will change and, by mass continuity, the meridional flow and thus the THC will change accordingly. This process, with typical time scales of 10–100 yr (Stocker 2000), can cause a slowdown (Manabe and Stouffer 1997) or total collapse of the THC (Bryan 1986). THC variations can also be generated by changes in regional oceanic convection due to localized input of freshwater, changes in sea ice cover, and local changes in surface heat and freshwater fluxes (Stocker 2000). This process has time scales of 1–10 yr and is often poorly simulated in ocean models.

Decadal to multidecadal THC changes during the last 50 yr are also suggested by observed changes in North Atlantic convective activity (e.g., Dickson et al. 1996), Atlantic Ocean salinity changes (e.g., Belkin et al. 1998; Dickson et al. 2002; Curry et al. 2003), the position of the separated Gulf Stream (GS; Joyce et al. 2000), surface heat and freshwater fluxes (Marsh 2000), the overflow from the Nordic seas (Hansen et al. 2001), and sea surface height (Häkkinen and Rhines 2004). Such oscillations are also found in several fully coupled general circulation models (CGCMs; e.g., Delworth et al. 1993; Knight et al. 2003; Cheng et al. 2004; Hu et al. 2004). For example, Delworth et al. (1993) showed that the THC in the Geophysical Fluid Dynamics Laboratory (GFDL) CGCM oscillates irregularly at approximately 50-yr time scales resulting mainly from ocean density anomalies in the North Atlantic sinking region, with sea surface temperature anomaly patterns resembling those of observed multidecadal variability in the North Atlantic. Further studies suggest that this THC oscillation is a mode of the fully coupled system (Weaver and Valcke 1998), with low-frequency surface heat flux forcing from the atmosphere as the main cause, especially that associated with the NAO (Delworth and Greatbatch 2000). Cheng et al. (2004) show that multidecadal (25–30 yr) oscillations exist in a CGCM with surface air–sea heat fluxes as a likely forcing.

In simulations with increased CO_2 levels, the THC weakens in most CGCMs, including the GFDL model (Manabe and Stouffer 1994; Dixon et al. 1999, 2003; Stouffer and Manabe 2003), the Hadley Centre GCM (HadCM3; Wood et al. 1999), the National Aeronautics and Space Administration (NASA) Goddard Institute of Space Studies (GISS) model (Russell and Rind 1999), the Canadian model (Boer et al. 2000), a Hamburg model (ECHAM3/LSG;Voss and Milkolajewicz 2001), and the National Center for Atmospheric Research (NCAR) Parallel Climate Model (PCM; Dai et al. 2001a; Hu et al. 2004). The THC also weakens in several intermediate-complexity models in response to increased CO_2 (e.g., Stocker and Schmittner 1997; Rahmstorf and Ganopolski 1999; Schmittner and Stocker 1999; Wiebe and Weaver 1999). On the other hand, the THC changes little in a few CGCMs, including a Hamburg model (ECHAM4/OPYC3; Latif et al. 2000), the NCAR Climate System Model (CSM 1.3; Gent 2001), and the GISS AGCM coupled to a hybrid coordinate ocean model (Sun and Bleck 2001). Most of these CGCMs, except the HadCM3, CSM, PCM, and GISS models, use surface flux adjustments.

A stable THC in response to increasing CO_2 was possible in the ECHAM4/OPYC3 because salty surface water was advected into the North Atlantic sinking region, which compensates the effects of local warming and freshening (Latif et al. 2000). In the CSM, the northwest Atlantic became warmer and more saline with little change in surface ocean density (Gent 2001). Sun and Bleck (2001) also found that the THC stability was maintained by a salinity increase that counteracts the thermal effect of surface warming. In the models producing a weakened THC, both the freshening effect of increased precipitation and river runoff and the thermal effect of local warming on surface ocean density play a role, although their relative importance during different stages of the weakening varies with individual models (Dixon et al. 1999; Mikolajewicz and Voss 2000; Cubasch et al. 2001). The freshwater forcing is expected since increased precipitation at northern mid- and high latitudes is a common response of most CGCMs to increased greenhouse gases (Cubasch et al. 2001). Many CGCMs also produce surface warming over the North Atlantic Ocean under increased CO_2; the thermal effect is thus also expected. Some coupled CGCMs, however, produce little warming (e.g., Wood et al. 1999; Boer et al. 2000) or substantial cooling (Russell and Rind 1999; Dai et al. 2001a) over the North Atlantic sinking region at the time of CO_2 doubling. In these cases, the local thermal effect is negligible or even works to enhance the THC in the cooling cases. Nevertheless, all these models produce a weakened THC.

Here we analyze the unforced variations in the Atlantic THC and the associated changes in horizontal ocean currents in a 1200-yr control run, and compare the unforced variability to those in simulations of the twenty-first- and twenty-second-century climates under projected emissions scenarios using a nonflux-corrected CGCM, namely the PCM (Washington et al. 2000). The PCM differs from many other CGCMs in that it uses a relatively high-resolution ocean model (~2/3° mean grid size) with a displaced North Pole that simulates the ocean currents in the North Atlantic and the Arctic Ocean realistically (Washington et al. 2000). We find that the THC has large oscillations around a 24-yr time scale that arise from the differential effects of THC-induced variations in surface ocean temperature and salinity on ocean density in the North Atlantic sinking regions, and that the THC weakens by ~12% during the twenty-first century and continues to weaken by additional ~10% in the twenty-second century if CO_2 keeps rising, but stabilizes if CO_2 levels off.

In the following, we first describe the model, spinup processes, and simulations in section 2. In section 3, we describe the THC variations and associated changes in ocean currents and surface fields in the 1200-yr control run. Section 4 is an analysis of observed variations in sea surface temperature (SST) and sea ice in comparison with the model simulation. The THC changes and processes involved in the twenty-first- and twenty-second-century simulations are discussed in section 5. Section 6 is a discussion of our results. A summary is given in section 7. Our focus here is on basinwide variations and changes. More detailed regional analyses have been reported in Hu et al. (2004).

2. Model and simulations

The PCM is a fully coupled climate system model consisting of an atmospheric general circulation model (GCM), an ocean GCM, a land surface model, and a dynamic–thermodynamic sea ice model (Washington et al. 2000). The PCM does not use flux adjustments and has a relatively high resolution (T42 or ~2.8° and 18 levels for the atmosphere and ~2/3° and 32 levels for the oceans). It produces a stable climate under current conditions that is comparable to observations (Washington et al. 2000; Dai et al. 2001b) and has near-observed El Niño amplitude (Meehl et al. 2001). In particular, the PCM's ocean GCM, which is the Los Alamos National Laboratory Parallel Ocean Program (POP; Smith et al. 1992; Dukowicz and Smith 1994), produces realistic ocean circulations in the North Atlantic and the Arctic Oceans as a result of relatively high resolution there and a displaced North Pole over North America (Washington et al. 2000). The PCM has been used to simulate the twentieth-century climate using various combinations of greenhouse gas, sulfate aerosol, solar, and volcanic forcing (Dai et al. 2001a; Meehl et al. 2003; Ammann et al. 2003) and the climate response to projected CO_2 and other emissions forcing in the next 1–2 centuries (Dai et al. 2001a,b,c).

Initialization of the PCM is described by Dai et al. (2004). The atmospheric and land models were run 10 yr from a standard 1 September initial condition (with solar irradiance and atmospheric CO_2 and other trace gases being set to values appropriate for 1870 conditions) using Levitus SST climatology (Levitus and Boyer 1994; Levitus et al. 1994) as the lower boundary condition. The last 5 yr were used to generate the atmospheric forcing data for the ocean and sea ice models, which were run 85 yr with an initial ocean state from the Levitus climatology and sea ice deduced from the Levitus SST (Boville and Gent 1998). During this ocean-alone integration, deep oceans were accelerated toward equilibrium using techniques described in Bryan (1984) and Danabasoglu et al. (1996). Using a state from the ninth year of the atmosphere-alone run and a consistent ocean state from year 84 of the ocean- and sea ice–alone run, the PCM was run in a fully coupled mode for about 1200 yr (without the deep ocean acceleration) with solar irradiance and atmospheric CO_2 and other trace gases fixed at 1870 levels. The THC was stable during the last three decades of the spinup run. In the 1200-yr coupled integration, there are small but steady trends in global, volumetrically averaged ocean temperature (-0.05°C century^{-1}) and salinity ($+0.001$ 24 ppt century^{-1}), which are considerably smaller than in some other CGCMs (e.g., Cheng et al. 2004).

Ensemble climate change simulations under a business-as-usual (BAU) and a CO_2 stabilization scenario are described in Dai et al. (2001a,c). These simulations started from the various decades in the second century of the 1870 control run, and used observation-based greenhouse gas [CO_2, CH_4, N_2O, O_3, and chlorofluorocarbons (CFCs)] concentrations and historical SO_2 emissions for the 1870–1996 period (referred to as the historical runs, see Dai et al. 2001d). For 1997–2099, these concentrations and emissions were estimated using an energy-economics model under a BAU scenario, which is close to the mean of all projections under the latest Intergovernmental Panel on Climate Change (IPCC) emissions scenarios (Nakićenović and Swart 2000). The BAU scenario was extended (in one of the ensemble runs) to 2200 by assuming constant emissions

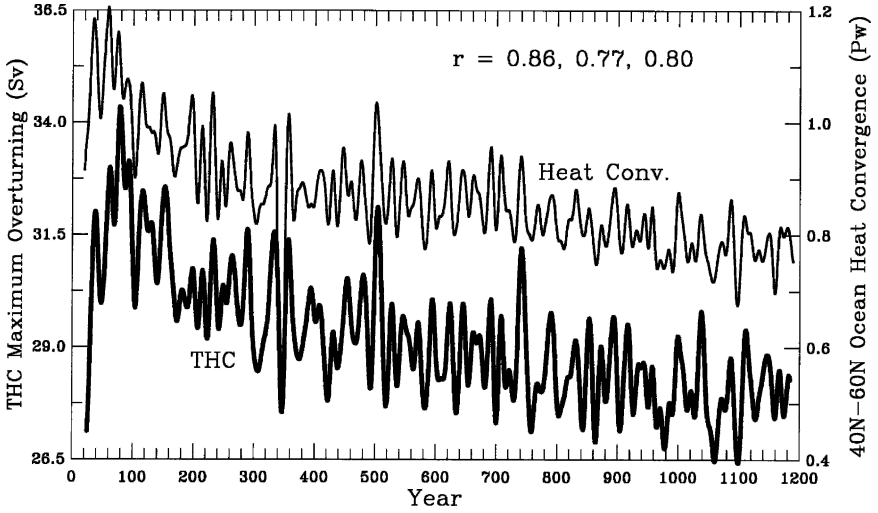

FIG. 1. Time series of the maximum THC streamfunction (annual mean and averaged over 32°–38°N and 1.1–1.6-km depth, cf. Fig. 4) (thick line, in Sv, 1 Sv $\equiv 10^6$ m^3 s^{-1}) and annual oceanic heat convergence within the top 1.5 km and 40°–60°N (thin line, in Pw, 1 Pw = 10^{15} W) from the 1200-yr control run. Variations on shorter than 15-yr time scales are filtered out. The three numbers inside the frame are the correlation coefficient, from left to right, between the two plotted curves, for variations on time scales between 15 and 100 yr, and for the THC leading the heat convergence by 1 yr for the band-passed correlation.

for CO_2, CH_4, N_2O, SO_2, and CFCs. The CO_2 level is ~710 ppm in 2100 and 1114 ppm in 2200 (see Dai et al. 2001c for more details and the simulated temperature and precipitation changes). In plots including the twenty-second century or the control run, we used only single runs; in all other plots we used five-member ensembles from the historical and twenty-first-century simulations. There were only small differences in the 30-yr-averaged fields between the single runs and the ensemble mean.

3. Atlantic THC in a 1200-yr control run

a. THC variations and associated changes in heat transport and ocean currents

Figure 1 shows the smoothed time series of the maximum strength of the THC, defined as the annual mean streamfunction averaged over 32°–38°N and 1.1–1.6-km depth (see Fig. 4 below), from the 1200-yr control run, together with the oceanic heat convergence between 40° and 60°N within the top 1.5-km depth in the North Atlantic Ocean (similar for SSTs over the same region). The initial strength of the THC was about 18 Sv (1 Sv $\equiv 10^6$ m^3 s^{-1}) at the time of coupling, which is close to current consensus estimates (e.g., Bryden and Imawaki 2001). It increased rapidly to ~34.5 Sv around model year 80, which is larger than any modern observations suggest. Thereafter, the THC weakened to ~30 Sv around year 170 and continued to weaken slowly in the subsequent centuries, although the decline rate leveled off after year ~1000 (Fig. 1). In addition, large multidecadal oscillations are evident in the THC and the heat convergence time series, which are discussed in detail in section 3b.

Figure 1 also shows that the heat convergence in the top 1.5-km midlatitude North Atlantic Ocean is strongly correlated, with almost no time lag, with the THC strength on decadal and longer time scales. Figure 2 shows that variations in the heat convergence come largely from changes in northward heat transport at 40°N (i.e., around the separated Gulf Stream path, see Fig. 4), which is higher during periods (e.g., years 80–84) when the THC is strong; whereas the changes at 60°N are small. Figure 2 also shows that the total meridional heat transport by the Atlantic Ocean in the PCM control run is comparable to current estimates from the equator to 40°N (Trenberth and Caron 2001), although the volume transport of the THC is too strong. The THC-induced heat convergence in the midlatitude North Atlantic Ocean warms the surface air not only in the Atlantic region (by 0.1°–0.3°C Sv^{-1} increase in the THC strength), but also over Europe (by 0.1°–0.2°C Sv^{-1}) and much of Asia (Fig. 3). Figures 2 and 3 confirm the notion that the poleward heat transport by the THC warms the extratropical North Atlantic and wind-downstream regions.

Figure 4 shows that the upper clockwise-flowing cell (i.e., the THC) in the Atlantic, which was stable during

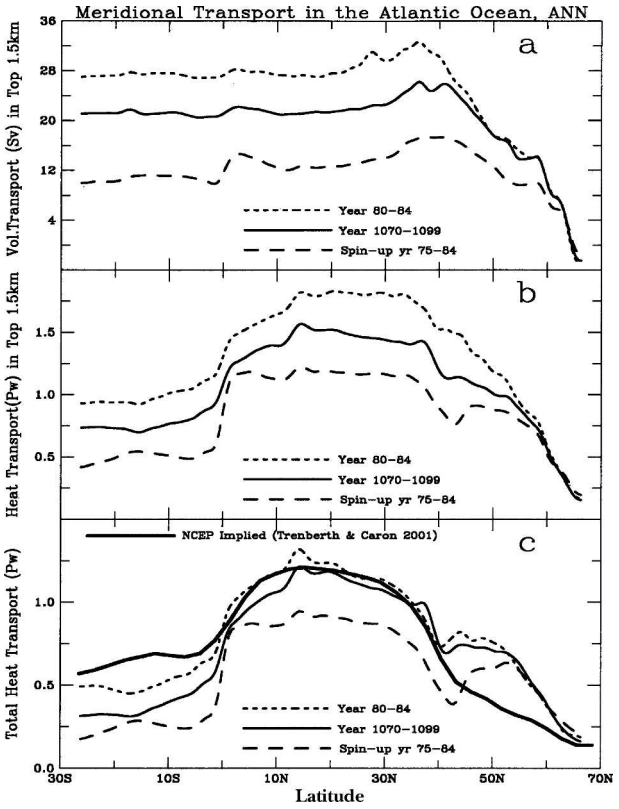

FIG. 2. Annual meridional transport of (a) volume (Sv) and (b) heat (Pw) within the top 1.5-km depth in the Atlantic Ocean for years 75–84 of the spinup run (i.e., just before the coupling, long dashed), years 80–84 (short dashed), and 1070–99 (thin solid) of the control run. (c) Same as (b) but for the heat transport with the entire Atlantic basin. Also shown (thick solid line) is the NCEP–NCAR atmospheric reanalysis implied Atlantic heat transport, which agrees overall with direct measurements except for south of ~20°S where the implied transport is too high (Trenberth and Caron 2001).

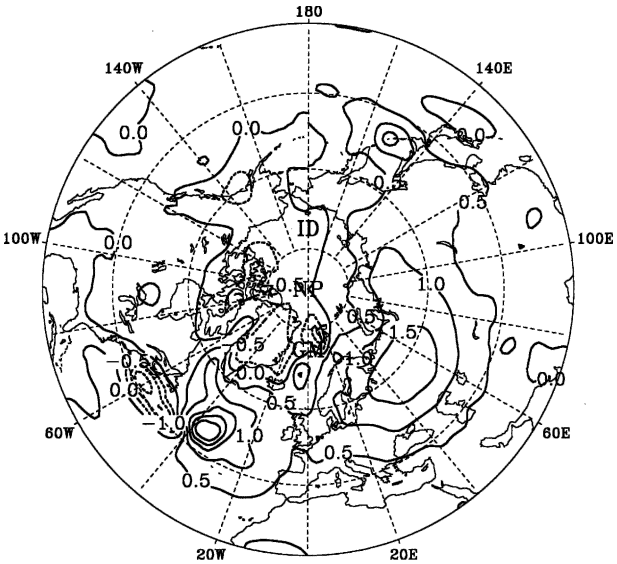

FIG. 3. Regression coefficients (at zero lag, 0.1°C Sv^{-1}) between the annual THC index (from Fig. 1) and annual surface air temperature north of 20°N during years 200–1199 of the PCM control run. The time series were detrended and variations on shorter than 10-yr time scales were removed before the regression analysis.

the last three decades of the ocean- and sea ice–alone spinup run, gained strength and depth rapidly during the first 80 yr of the coupled integration, while the bottom anticlockwise-flowing cell [i.e., the Antarctic Bottom Water (AABW)], weakened and disappeared by years 80–84. The depth of the maximum streamfunction deepened from around 1200 to 1600 m during this period as the whole upper cell expanded downward to cover the entire basin. As the strength of the THC decreased after year ~80 (Fig. 1), the THC became increasingly shallow and weak, with the maximum transport decreasing to ~28 Sv in 1070–99; while the bottom cell reemerged and gained both depth and strength (Fig. 4c).

Accompanying the changes in the strength and vertical extent of the THC, Atlantic upper-ocean currents also show large variations (Figs. 4d–f). Although the separation point of the Gulf Stream (GS) from the coast (around Cape Hatteras) varies little, there are considerable south–north shifts of the separated GS path in the open ocean, which is consistent with recent observations (Joyce et al. 2000). Specifically, the separated GS moves southward when the THC is strong (Fig. 4e) and northward when the THC is weak (Figs. 4d,f), while the path of the North Atlantic Current (NAC) moves westward (for strong THC) and eastward (for weak THC). During the strong THC periods (e.g., Fig. 4e), a very large portion of the NAC directly converges into the Labrador Sea, thereby contributing to the enhanced deep-water formation there. Since the subtropical water carried by the GS and the NAC has much higher temperature and salinity than the subpolar water, these horizontal current movements induce large temperature and salinity changes around the paths of the GS and NAC, as shown below.

Figure 4 is qualitatively consistent with Zhang and Vallis (2005, manuscript submitted to *J. Phys. Oceanogr.*, hereafter ZV), who found that the bottom vortex stretching induced by a downslope Deep Western Boundary Current (DWBC) leads to the formation of the northern recirculation gyre (NRG), which keeps the GS separated from the North American coast north of ~40°N. The results of ZV suggest that a strong THC with a strong DWBC should result in large bottom vortex stretching and thus a strong NRG that pushes the

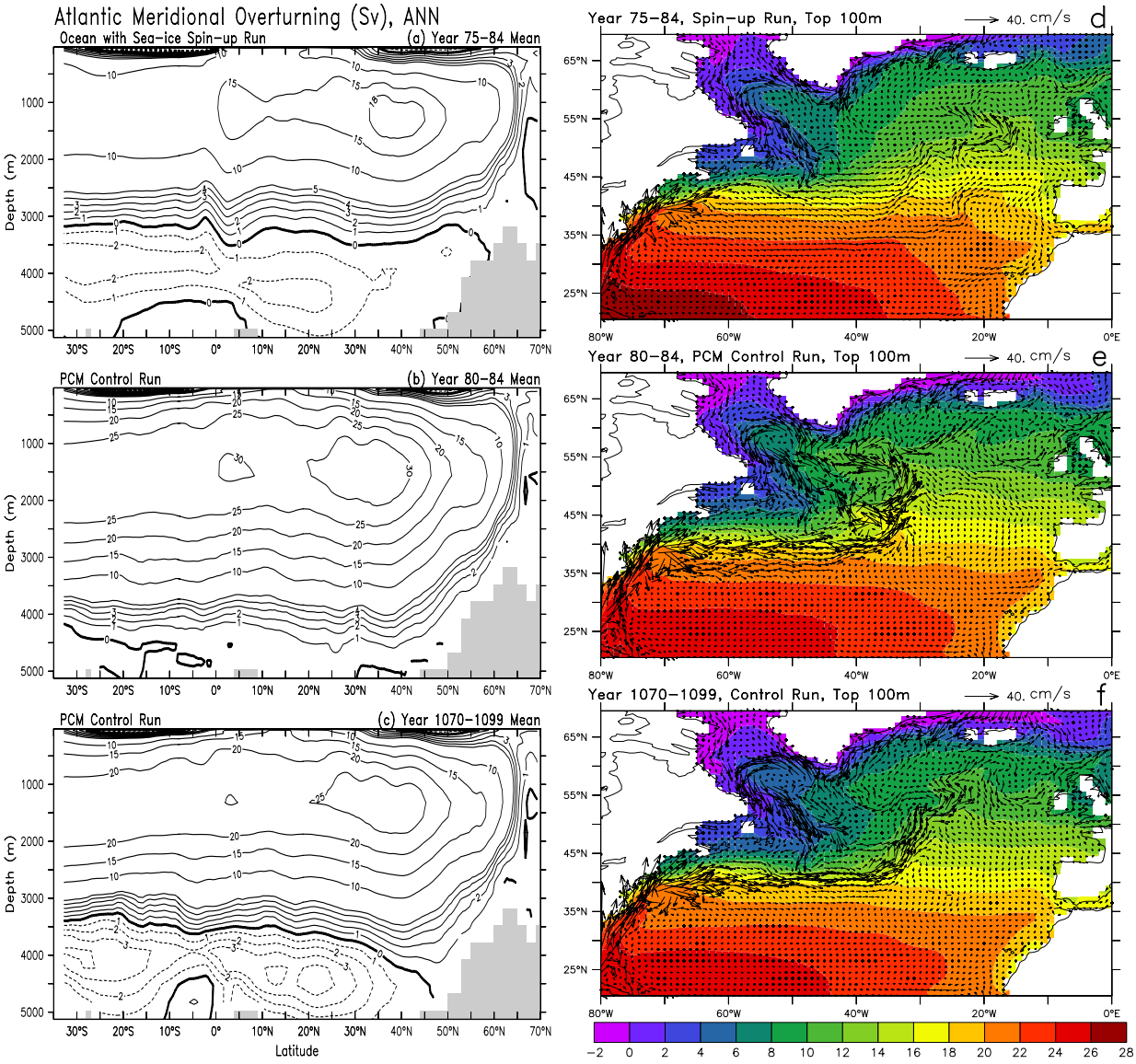

FIG. 4. (left) Zonally averaged annual meridional overturning streamfunction (Sv) for the Atlantic Ocean from (a) the ocean- and sea ice–alone run years 75–84 (just before the coupling), and from the coupled PCM control run for model years (b) 80–84 and (c) 1070–99. (right) SST (color, °C) and top 100-m-averaged ocean currents (arrows) in the North Atlantic Ocean simulated by the PCM from (d) the ocean- and sea ice–alone run years 75–84, and during the control run at years (e) 80–84 and (f) 1070–1099.

separated GS path southward, and vice versa for a weak THC. Their results also show that the NAC is more west–east orientated when the GS path is shifted northward than when the GS is to the south, consistent with the NAC variations shown in Figs. 4d–f.

The strengthening of the THC during the first 80 yr of the control run is caused by the large cooling in the upper Atlantic Ocean after the coupling. This cooling more than compensates the effect of moderate freshening (south of ~40°N) and results in large increases in upper-ocean density (not shown). During the subsequent centuries of the control run, however, the freshening effect becomes increasingly more important than the cooling effect on the density in the upper Atlantic Ocean, resulting in decreases in upper-ocean density and thus the THC. The salinity decreases in the upper ocean are caused by increases in net freshwater flux into the ocean (not shown). These density-induced THC changes provide analogs to greenhouse gas–induced THC changes since the greenhouse gas–

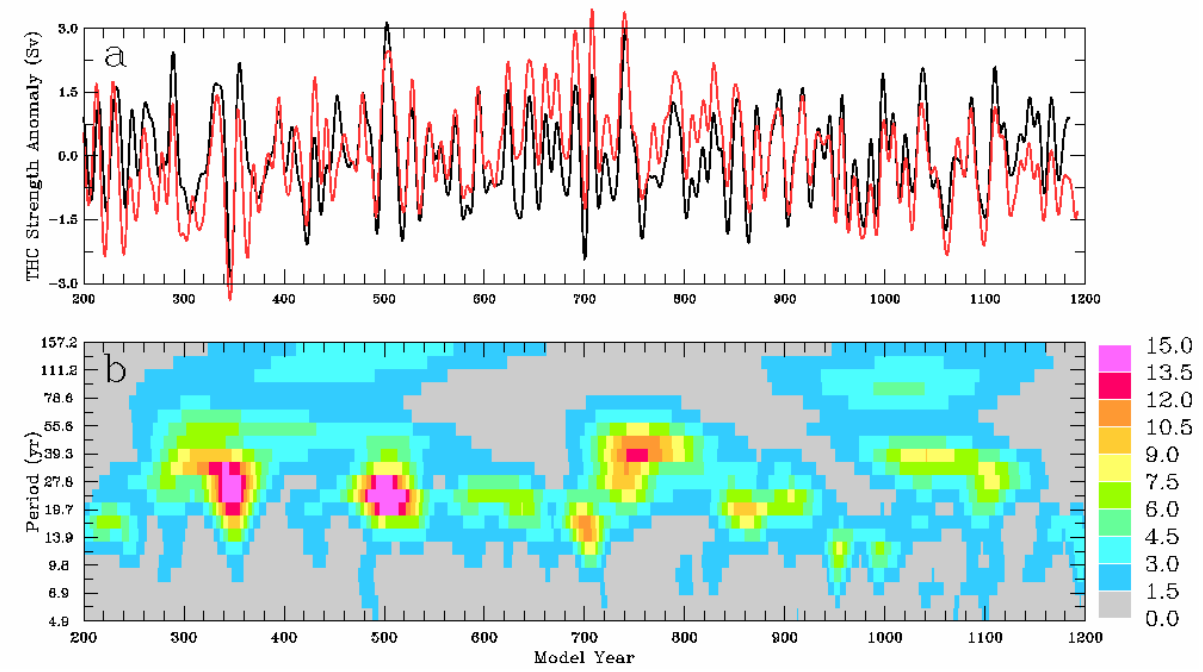

FIG. 5. (top) Detrended time series of the maximum THC streamfunction anomaly (Sv, black line) and volume transport within top 1-km depth at 40°N in the Atlantic Ocean (Sv, red line) with variations shorter than 10-yr time scales being removed. The curves have a maximum correlation of 0.70 at a zero time lag. (bottom) The time-period distribution of relative power of the detrended (unsmoothed) annual maximum THC streamfunction from a wavelet analysis.

induced warming also decreases upper-ocean density (see section 5).

b. A 24-yr oscillation in the THC and other fields

Both wavelet (Fig. 5b) and traditional (Fig. 6a) spectral analyses show that the strength of the THC varies mainly on 15–40-yr time scales after removing the linear trends associated with the slow adjustments in the PCM control run. While irregular and varying with time, these variations exhibit oscillatory nature with mean-peak amplitudes around 1.5–3.0 Sv (Fig. 5a) and a sharp peak around 24 yr (Fig. 6a). This peak is stronger during the first 800 yr than the last 400 yr of the control run. There is very little power on time scales shorter than 10 yr (Fig. 5b); the spectrum is a red noise with a lag-1 correlation of 0.4.

Also shown in Fig. 5a (red line) is the northward volume transport within the top 1-km depth at 40°N in the Atlantic Ocean. This transport serves as an alternative THC index (Gent 2001). Figure 5a shows that the two indices are strongly correlated ($r = 0.7$) on multidecadal time scales. Furthermore, the correlation is strongest at a zero time lag, suggesting that the results regarding the time lags between the THC streamfunction index and other fields discussed below are insensitive to the choice of the THC index.

The spectrum of the NAO index (defined in the caption of Fig. 6) also shows the strongest peak around 24 yr that is well above the white noise level. The NAO index, which is a measure of a major air–sea interaction mode (i.e., the NAO) in the North Atlantic region (Hurrell 1995), is essentially a white noise with a few significant peaks (Fig. 6b). Figure 6 suggests that the 24-yr oscillation in the THC is coupled to the atmosphere over the North Atlantic Ocean. [Figure 9a (thick line) shows that the December–March NAO index leads the annual THC index by about 1 yr, which indicates the air–sea coupling is almost simultaneous.]

To further examine this 24-yr signal in other related fields, we performed empirical orthogonal function (EOF) analyses of North Atlantic annual SST, sea surface salinity (SSS), surface ocean density, surface net energy flux, surface net water flux [i.e., evaporation (E) minus precipitation (P)], and sea ice fraction. We found that the signal of the THC index, including the 24-yr oscillation, is evident in the leading EOFs of all these fields (Figs. 7–8). Figure 7 shows the EOF spatial patterns of these fields whose temporal coefficients or principal components (PCs) are clearly correlated with

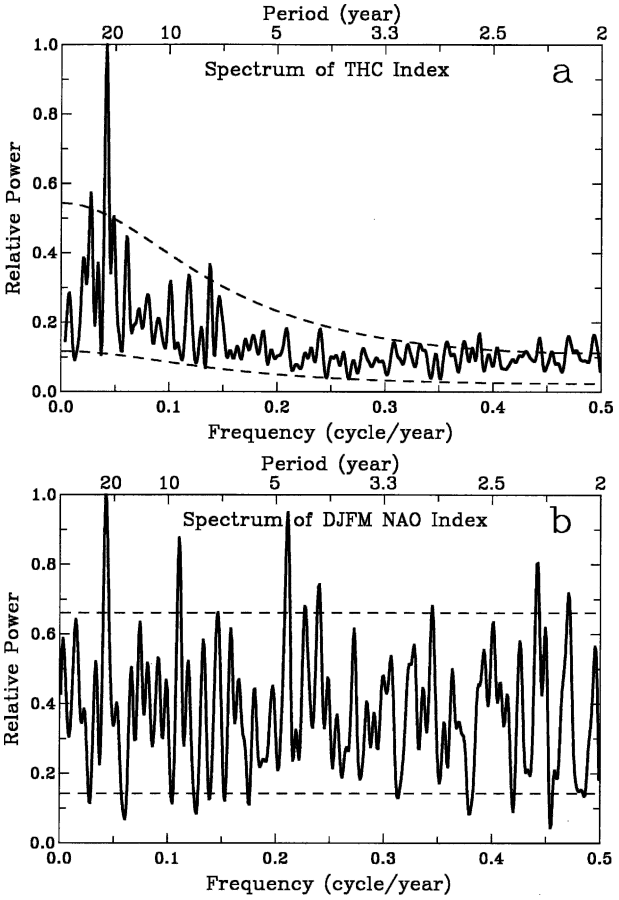

FIG. 6. Power spectrum of (a) the annual maximum THC time series shown in Fig. 1 (detrended but without the smoothing, for years 176–1199) and (b) the NAO index, from the control run, which is the difference of the normalized DJFM sea level pressure anomalies between Lisbon, Portugal (38.8°N, 9.1°W), and Stykkisholmur, Iceland (65.1°N, 22.7°W; as in Hurrell 1995). The dashed lines are the 95% and 5% confidence limits. The largest peak is at 23.8 yr for both (a) and (b).

the THC index (Fig. 8), with the THC leading the SST, *E–P*, and the other fields by 2–3 yr on multidecadal time scales (Fig. 9a, other variables in Fig. 8 have lag correlations with the THC similar to that for SST). This time lag suggests that the THC multidecadal oscillations induce the variations in the surface fields.

The EOF patterns (Fig. 7) show that the SST is colder than normal in the Labrador Sea and most midlatitude North Atlantic Ocean but warmer around 39°–44°N, 40°–67°W when the THC is weak. This SST change pattern results from the horizontal changes in the Atlantic currents (cf. Figs. 4d–f); namely, the separated GS path is shifted northward and the NAC moves eastward when the THC is weak, thereby causing a change of water type (subtropical versus subpolar) and thus the SST and SSS changes. The SSS changes are, however, modulated by surface net water flux ($E - P$; Fig. 7e), which is influenced by lower-tropospheric changes (stability, cloudiness, etc.) that are largely induced by the SST changes. The $E - P$ pattern resembles that of the surface net energy flux (Fig. 7d, positive upward) and both show negative (positive) anomalies west (east) of ~30°W in the midlatitude Atlantic Ocean when the THC is weak. Sea ice increases around the Labrador Sea and decreases between Iceland and Greenland, which is broadly consistent with the SST changes. Surface ocean density change patterns result from the relative contributions of the SST and SSS changes, with the SSS influence predominating around the separated GS path and east of ~30°W and the SST changes being more important west of ~30°W (Fig. 7c).

The THC-induced SST and SSS variations produce density oscillations that are correlated with the THC index with time lags (Fig. 9b), similar to Delworth et al. (1993) but with shorter time scales. Specifically, both the SST- and SSS-induced density variations (mostly in the midlatitude North Atlantic) lag the THC index by 2–3 yr but with opposite signs. The net effect of the SST and SSS results in strongest negative (positive) correlations between the surface density and the THC strength approximately 5–6 yr after (before) the THC peaks. The phase relationship between the 24-yr oscillations of the THC and the midlatitude North Atlantic upper-ocean density is illustrated in Fig. 10. During the first 12 yr of a cycle, positive density anomalies lead to increases in NADW formation and THC's strength; during the next 12 yr, negative density anomalies weaken the THC (Fig. 10). On the other hand, the THC-induced SST and SSS changes cause the density to change (Fig. 9), but the combination of the SST and SSS effects on density results in the phase relationship shown in Fig. 10 (i.e., density leads THC by ~90° in phase), which provides the mechanism for the THC to oscillate.

A composite density-difference map (Fig. 11a), together with its vertical structure (Fig. 11b), shows that most midlatitude North Atlantic upper oceans have above-normal density 6 yr before the THC peaks. Figure 11b shows that the deep-ocean density in the Atlantic basin is below normal when the THC is strong. This is consistent with variations in the relative strength of the upper and lower cells of the Atlantic meridional overturning circulation (MOC; Figs. 4a–c). Specifically, when the THC is strong, it extends downward while the AABW retreats southward. As the AABW has higher density than the NADW, this change of water mass

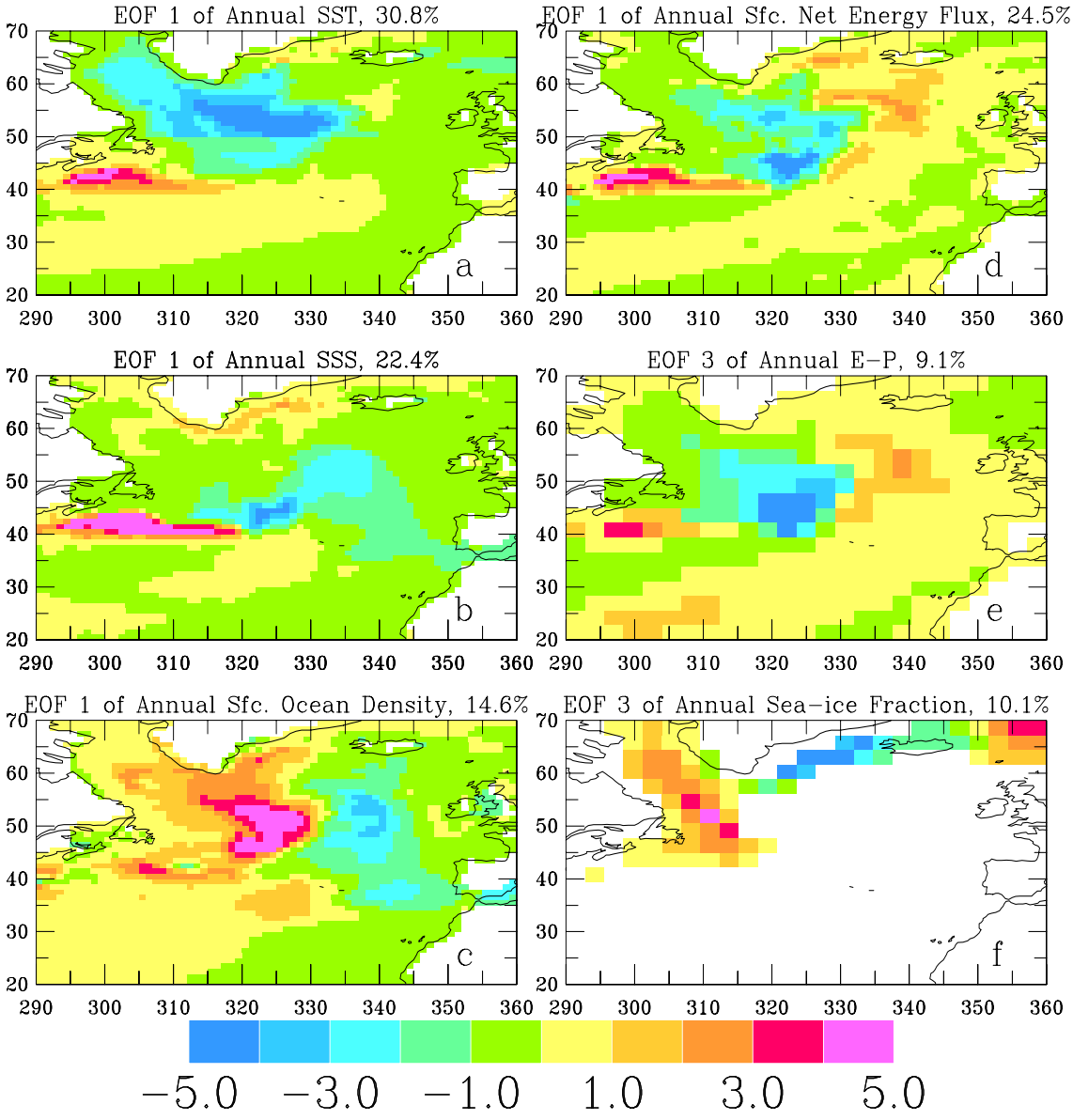

FIG. 7. The EOFs of North Atlantic annual (a) SST, (b) SSS, (c) surface ocean density (all density fields in this study are referenced to 2-km depth, i.e., σ_2 is used), (d) surface net energy flux, (e) surface $E - P$, and (f) sea ice fraction whose temporal coefficients (Fig. 8) are correlated with the THC index (cf. Fig. 1) during the PCM control run. The percentage variance explained by the EOF is shown at the top of each panel. Note that the EOFs and the PCs in Fig. 8 are plotted in a way that the variables would have negative (positive) anomalies over the blue areas when the THC is weak (strong).

induces a density decrease in the deep ocean from a weak THC to a strong THC.

4. Comparisons with observed SST and sea ice variations

To find out whether the above PCM-simulated variations have any resemblance to the real world, we analyzed the observation-derived SST and sea ice concentration data (sufficient sampling only after 1953 for sea ice) obtained from the Hadley Centre Sea Ice and SST (HadISST) dataset (Rayner et al. 2003). Figure 12 shows that the first and second EOFs of the 1953–2003 winter [December–March (DJFM)] SST and sea ice data, with their PCs shown in Fig. 13. The time series of the first EOF of the SST, which is consistent with an analysis of 1900–89 data (Deser and Blackmon 1993), strongly correlates with Northern Hemispheric (r =

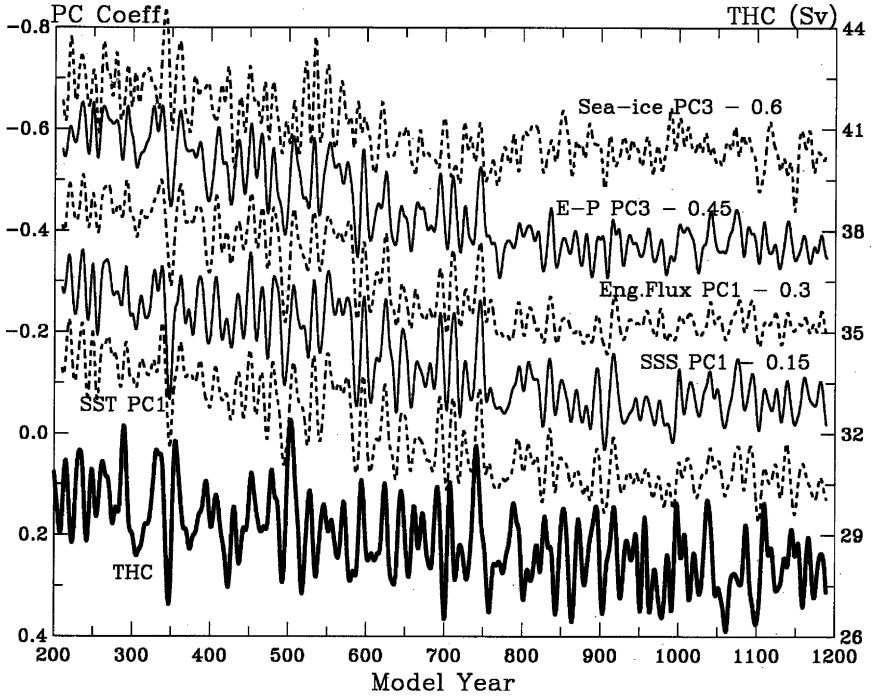

FIG. 8. The temporal coefficient or PC (left coordinate, shifted by the amount indicated) of the EOFs shown in Fig. 7, together with the THC index (bottom solid curve, right coordinate). Variations on shorter than 10-yr time scales are filtered out. The product of the PC and EOF (of Fig. 7) has the physical unit of the variable.

0.79; Fig. 14) and global-mean (r = 0.72, not shown) surface air temperature, even extending back to 1900. This suggests that the first EOF of the SST, with relatively large multidecadal amplitudes that have been discussed by Kushnir (1994) based on data up to the late 1980s, is associated with the trends and multidecadal variations in the global and hemispheric mean temperatures. Considering that the North Atlantic (cf. Fig. 12) is only a very small fraction of the global and Northern Hemispheric surface, this correlation, which has not been pointed out before to the best of our knowledge, is remarkable. This EOF suggests that the SST in the midlatitude North Atlantic has warmed substantially in phase with the global-mean temperature during the twentieth century, and the warming rates are much faster since the late 1970s than before. Aside from accompanying salinity changes, this SST warming alone could potentially have reduced upper-ocean density around the Labrador Sea and other NADW formation regions, thereby slowing down the THC in the twentieth century. An analysis of surface heat and freshwater fluxes (Marsh 2000), however, suggests little change of NADW formation rates in the Labrador Sea from 1980 to 1997, although observations of sea surface height suggest that the Atlantic subpolar circulation has weakened during the 1990s (Häkkinen and Rhines 2004), which would be consistent with a weaker THC (cf. Figs. 4d versus 4e).

The first EOF and its PC of the sea ice concentration is roughly consistent (with a slight time lag) with the first mode of the SST. Specifically, sea ice concentration around the southern Greenland coastal lines and in the Davis Strait and Labrador Sea increased from 1953 to 1972 when the SST decreased; thereafter, sea ice has been diminishing as the SST warms rapidly since the late 1970s (Figs. 12–13).

The second EOF of the SST and sea ice has been discussed extensively in a number of previous studies (e.g., Deser and Blackmon 1993; Deser et al. 2000, 2002). These SST and sea ice patterns result from surface wind (and resulting surface air temperature) changes associated with the NAO, which is correlated with the PCs of the second EOF of the SST and sea ice (Fig. 13).

The THC-associated EOF of SST and sea ice in the PCM (Figs. 7a,f) broadly resembles the second EOF of observed SST and sea ice (Fig. 12), respectively. For example, peak SST anomalies of opposite signs are seen around the 50°N central Atlantic and 40°N western Atlantic in both the PCM and observations. Sea ice

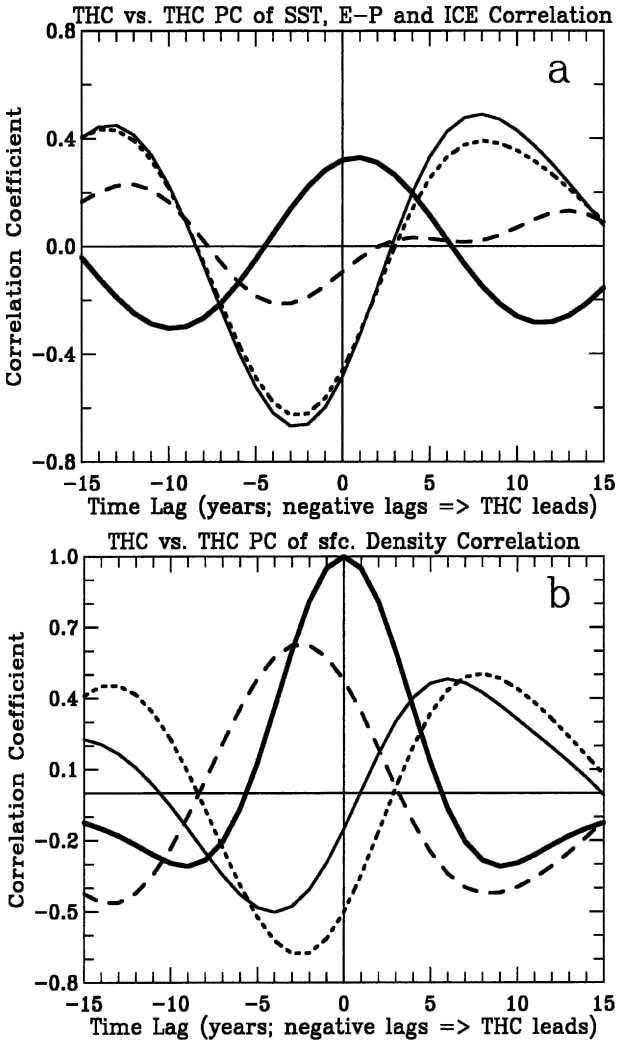

FIG. 9. (a) Lag correlation coefficients between the bandpass-filtered (time scales = 10–50 yr) THC index and PC of SST (thin solid line), $E - P$ (short dashed), and sea ice fraction (long dashed) shown in Fig. 8 (see Fig. 7 for the spatial domain). Also shown (thick solid) is the lag correlation coefficient between the bandpass-filtered (time scales = 10–30 yr) THC index and the NAO index. A negative (positive) lag indicates that the THC leads (lags) the other variable by the lag time. (b) Same as (a) but for THC vs the leading PC of surface ocean density correlation (time scales = 10–50 yr): thin solid line is for density including both temperature (T) and salinity (S) effects, short-dashed line for density due to T only, and long-dashed line for density due to S only. A positive correlation indicates that the surface density in the 45°–60°N Atlantic Ocean is above normal during strong THC periods. For reference, the THC vs itself correlation is also shown as the black solid line.

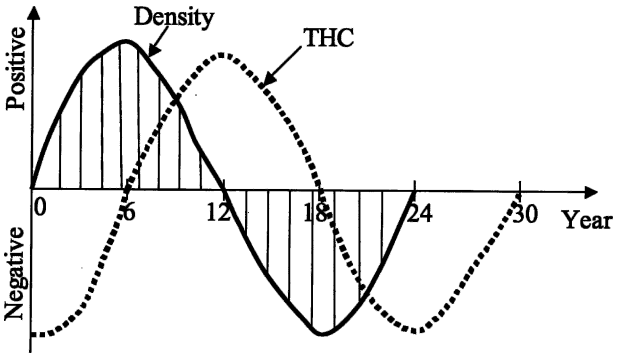

FIG. 10. A schematic diagram showing the phase relationship of the 24-yr oscillations in the Atlantic THC strength (dashed line) and midlatitude North Atlantic upper-ocean density (solid line). Note that the THC strength increases (decreases) when the density anomalies are positive (negative).

anomalies are out of phase around the west and east coasts of southern Greenland in both the PCM and data, although regional differences exist. These similarities, combined with the peak power of the NAO index at the 24-yr time scale (Fig. 6) and the correlation between the THC and NAO (Fig. 9a), suggest that the 24-yr oscillation in the THC is strongly coupled to the NAO in the PCM. The fact that the THC leads the SST and other surface fields (Fig. 9) suggests that the THC is likely a cause for the 24-yr peak variability in the NAO. This does not, however, exclude the possibility that the near–white noise flux forcing associated with the NAO (Fig. 6b) could provide an energy source for the multidecadal THC oscillations. It should be noticed that the 24-yr time scale is longer than the time scales with peak power in 1900–2003 DJFM SST PC2 (~13 yr) and 1900–2003 NAO index (~8 yr). This is not surprising as the ocean acts as an integrator of atmospheric forcing.

5. Ocean circulation changes in projected future climates

In this section, we discuss the PCM-simulated THC responses to projected future CO_2 and other anthropogenic forcing in the next two centuries. We found that the forced THC changes resemble some aspects of the THC variations in the control run, as ocean density changes are the direct cause for these changes in both cases.

Figure 15 shows the time series of the maximum streamfunction and northward volume transport within the top 1-km depth at 40°N in the North Atlantic Ocean over the 1950–2199 period from a historical run and a BAU run (thick line), a CO_2 stabilization run [dashed line, the CO_2 increase rate slows down after year ~2040 and becomes zero by 2150, see Dai et al. (2001c) for details], and the control run (for the corresponding

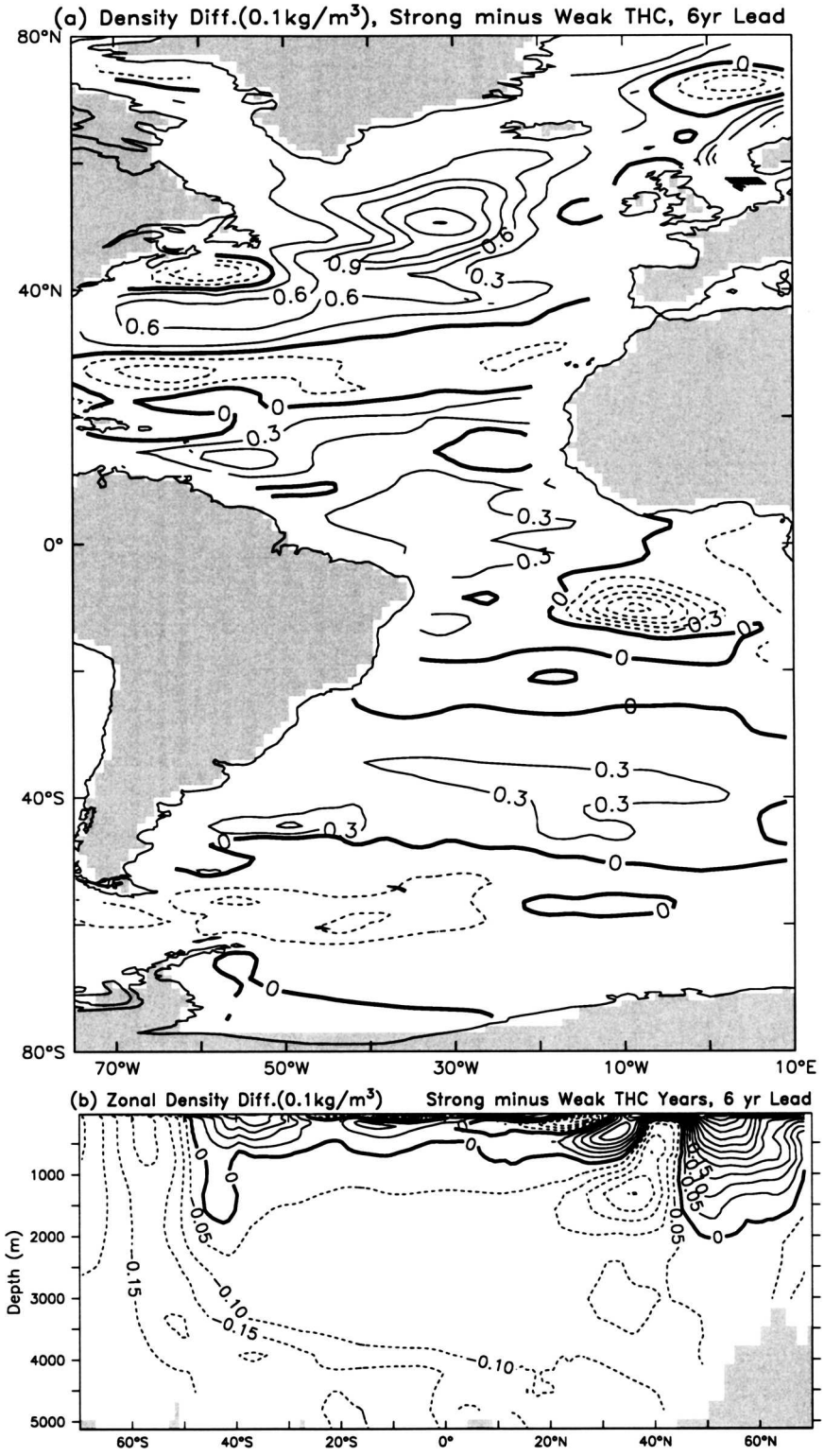

FIG. 11. (a) Top 100-m mean density difference (kg m^{-3}) between strong (anomaly above 1.5 std dev) and weak (below −1.5 std dev) THC years with the density leading the THC by 6 yr, e.g., year 740 is a strong THC year and density of year 734 is used. (b) Depth–latitude distribution of the zonal mean of the density difference shown in (a).

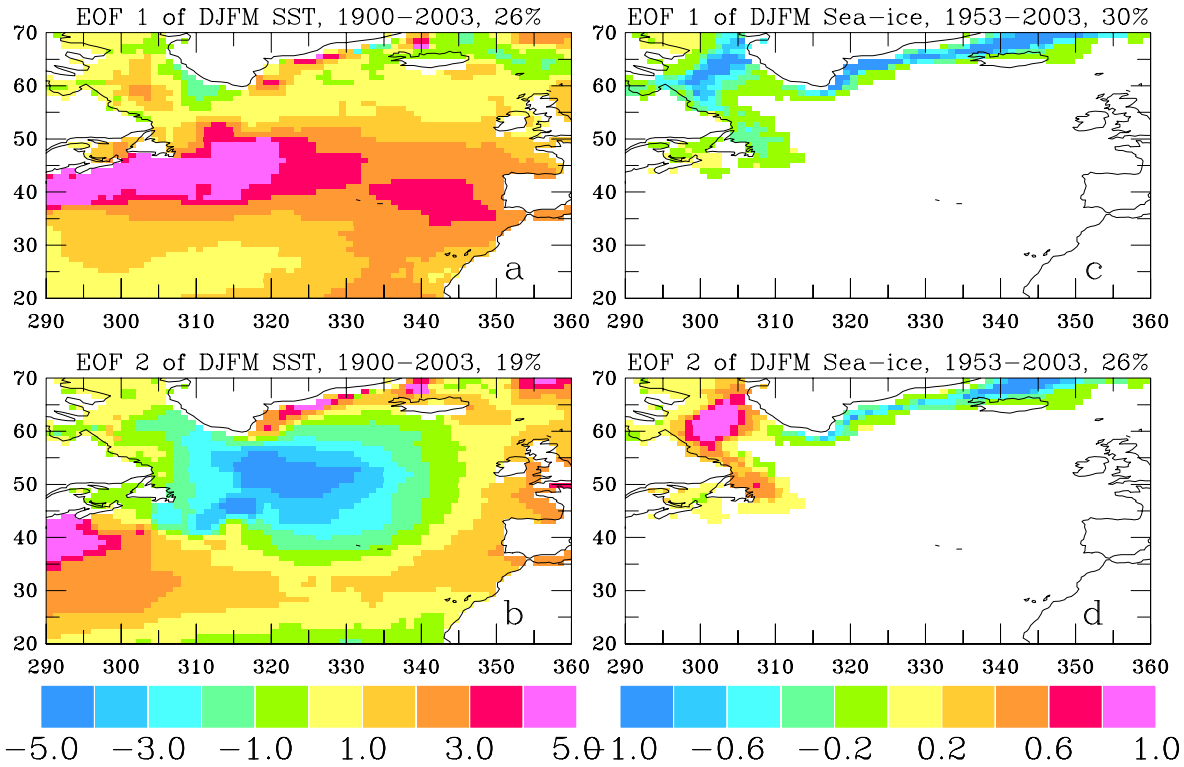

FIG. 12. The first and second EOFs of observed (left) DJFM SST during 1900–2003 (similar for 1953–2003) and (right) sea ice concentration during 1953–2003 over the North Atlantic (20°–70°N). The SST and sea ice data were from the HadISST1.1 dataset (Rayner et al. 2003). The explained percentage variance is shown on top of each panel.

model years, thin solid line). Both the maximum streamfunction and the transport at 40°N decrease steadily over the 250-yr period in the BAU run, while they decrease only in the twenty-first century and then stabilize during the twenty-second century in the stabilization run as atmospheric CO_2 stabilizes at 550 ppm (Dai et al. 2001c). On the other hand, trends in the control run over this 250-yr period are not evident, given the large multidecadal variations. In the BAU run, the interdecadal variations become smaller in the twenty-second century as the mean transports decrease. These results further confirm that in the PCM the Atlantic THC weakens significantly by ~12% (with northward heat transport around 40°N decreased by a similar amount) in response to projected CO_2 and other greenhouse gas increases during the twenty-first century. The THC could either stabilize at a weakened state if the greenhouse gases stabilize (which is consistent with Thorpe et al. 2001), or continue to weaken (by additional ~10%) if atmospheric CO_2 keeps rising in the twenty-second century.

Figure 16 shows the zonally averaged streamfunction for the annual mean MOC in the Atlantic Ocean for (Fig. 16a) 1970–99 from one historical run, (Fig. 16b) 2070–99, and (Fig. 16c) 2170–99 from one BAU scenario run. There was slight weakening (strengthening) of the upper (bottom) cell of the MOC during the corresponding model year period of the control run, and these unforced MOC changes were removed in Fig. 16. Even after the adjustment for the unforced drift, the MOC still changed substantially. The upper cell (i.e., the THC) became shallower and weaker, with the maximum transport decreasing from about 28 Sv in 1970–99 to 25 Sv in 2070–99 and to 23 Sv in 2170–99. The THC reached to the bottom of the basin in 1970–99 but retreated to above 3.5-km depth in 2170–99. At the same time, the bottom cell (i.e., the AABW) gained strength and expanded upward to ~3.5 km depth and northward to the northern midlatitudes (Fig. 16). These changes are qualitatively similar to those that occurred in the control run after the first century (cf. Figs. 4b,c), but at a much faster pace.

Similar to the control run (Figs. 4e,f), the THC's weakening in the simulated future climate was accompanied by an eastward shift of the NAC (Fig. 17). As noticed in section 3a, this horizontal circulation change

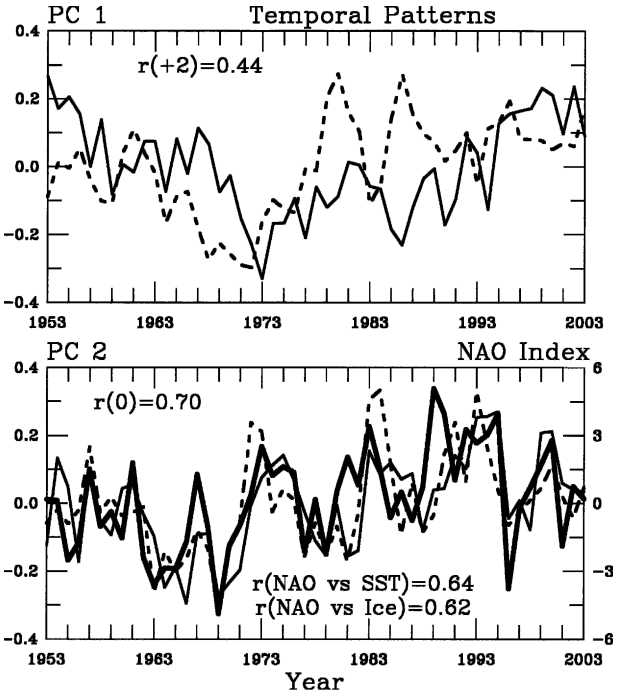

FIG. 13. Temporal coefficients of the (top) EOF 1 and (bottom) EOF 2 of observed DJFM SST (solid) and sea ice concentration (dashed) shown in Fig. 12. Also shown in the bottom panel is the NAO index (thick solid; from Hurrell 1995 and updates). The maximum correlation coefficient between the curves is also shown, with the sea ice leads the SST by (top) 2 yr and (bottom) zero lags.

resulted from reduced bottom vortex stretching induced by a weakened downslope DWBC (ZV) that was associated with a weak THC.

Surface wind changes (Fig. 18) and their implied Sverdrup transport (not shown) during the twenty-first century are consistent with the THC weakening. Figure 18 shows that a high pressure center and anticyclonic winds were developed over the central midlatitude North Atlantic, where sea surface temperatures became colder in 2070–99 than in 1970–99 (cf. Fig. 20a) because of the NAC path changes.

Zonally averaged density (referenced to 2-km depth) fields (Figs. 19a,d) show that upper-ocean density decreased more than in the deeper ocean during the twenty-first and twenty-second centuries, as the greenhouse gas–induced surface warming penetrated downward gradually (Figs. 19b,e). Furthermore, the density decreases in the North Atlantic sinking region (~45°–65°N, cf. Fig. 16), except for the region around 50°N where a cooling (cf. Fig. 20a) caused a density increase during the twenty-first century, were generally larger than in the southern end of the basin (south of 55°S). These density changes weakened the THC and allowed heavier AABW (with $\sigma_2 \geq 36.90$ kg m^{-3}) to penetrate north- and upward, thereby expanding the bottom cell while narrowing the THC. Salinity changes (Figs. 19c,f) were relatively small, except for the region where large ocean current changes occurred (cf. Fig. 17). The dependence of the THC strength on the south–north difference of density changes is consistent with Hughes and Weaver (1996) and Thorpe et al. (2001) who both found the strength of the THC is proportional to the meridional gradient of the steric height (equivalent to column-integrated density).

The above zonal mean density changes are consistent with the density change patterns in surface oceans (Figs. 20c,f). Figure 20 shows that, except for the cool-

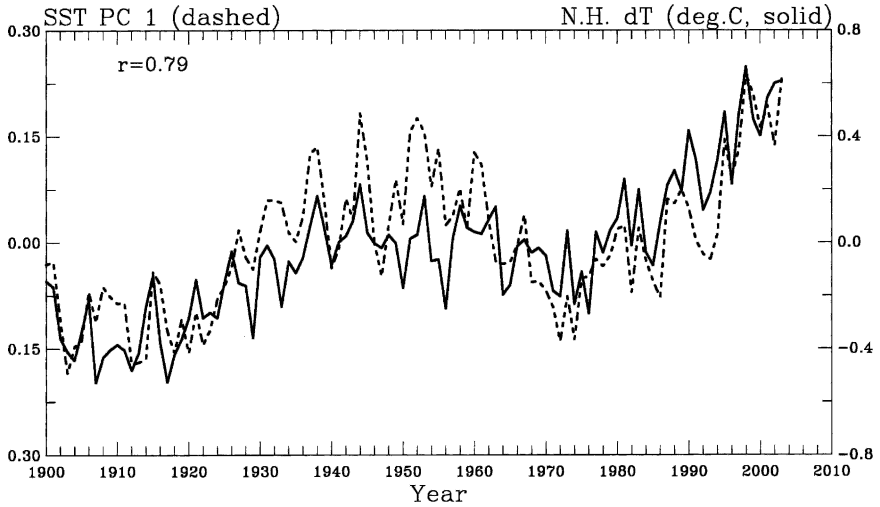

FIG. 14. The temporal coefficient (dashed) of the EOF 1 of observed North Atlantic (20°–70°N) annual SST during 1900–2003, together with Northern Hemispheric annual surface air temperature (from Jones and Moberg 2003). The correlation coefficient between the two is 0.79.

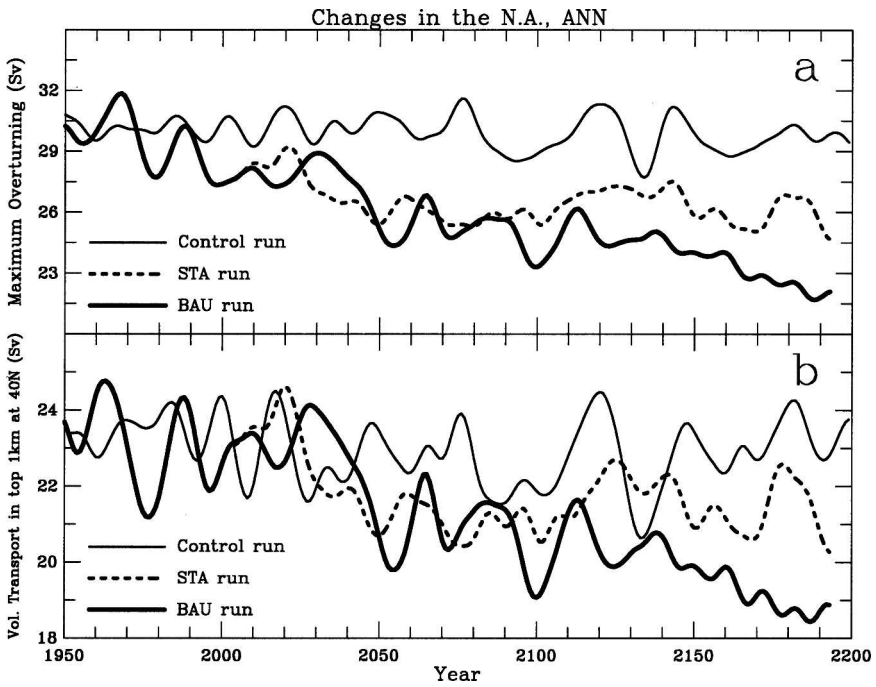

FIG. 15. Smoothed time series of the (a) maximum overturning (averaged over 32°–39°N and 1.1–1.6-km depth) and (b) northward volume transport within the top 1-km depth at 40°N in the North Atlantic Ocean for the control (thin), CO_2 stabilization (STA, dashed), and BAU (thick) cases. Only one run is used for each case.

ing region in the central midlatitude North Atlantic, upper-ocean density decreased by 0.2–0.4 kg m^{-3} over most of the northern mid- and high-latitude Atlantic basin, compared with decreases of 0.1 kg m^{-3} south of 60°S. Surface warming (Figs. 20a,d) was the major contributor to the density decreases in both the North Atlantic and Southern Ocean, although freshening around Greenland and Weddell Sea coasts (due to sea ice melting) was also a significant contributor. Salinity increases north of 45°N and south of 20°S in the Atlantic basin were small ($\leq$0.2 psu), thus allowing the thermal effect on density to dominate. The small salinity changes were consistent with small changes in surface $E - P$ as both E and P increased slightly over these regions (not shown).

Two exceptions are the central midlatitude North Atlantic, where both temperature and salinity decreased significantly, and a region around 39°–44°N, 40°–67°W, where both temperature and salinity increased substantially (Figs. 20a,b). As discussed above, these temperature and salinity changes result from the GS and NAC path changes (Fig. 17).

6. Discussion

Similar to the multidecadal oscillations shown in Fig. 5, Hu et al. (2004) also found an oscillation in the THC around a 20-yr time scale in a separate 300-yr control run by the PCM. The mean-peak amplitudes (1.5–3.0 Sv) and time scales (15–40 yr) of the THC oscillations reported here, as well as the associated surface temperature changes (Fig. 3), are close to those in the HadCM3 (Knight et al. 2003). The PCM-simulated THC oscillations are very comparable to those (amplitude = 2.0–2.5 Sv, periods = 25–30 yr) in the Miami Isopycnic Coordinate Ocean Model coupled to the NCAR CCM3 (Cheng et al. 2004). The 24-yr time scale also is comparable to the 20-yr THC oscillations found in an ocean GCM (Weaver et al. 1994). On the other hand, the GFDL model showed THC quasi oscillations with amplitudes of 1–2 Sv at longer time scales (~40–60 yr) (Delworth et al. 1993). The large 24-yr oscillation seen in the PCM supports the notion of decadal climate predictability over the North Atlantic region (Griffies and Bryan 1997).

Simplified model studies suggest that the preferred periodicity in the ocean is determined by the advective velocity (which relates to the advective mechanism) in the upper ocean and the time scales of low-frequency atmospheric variability (Saravanan and McWilliams 1998), and for the North Atlantic Ocean it is around 16–20 yr and is partially excited by atmospheric forcing (Saravanan et al. 2000). Coupled GCM investigations (e.g., Delworth and Greatbatch 2000) suggest that the

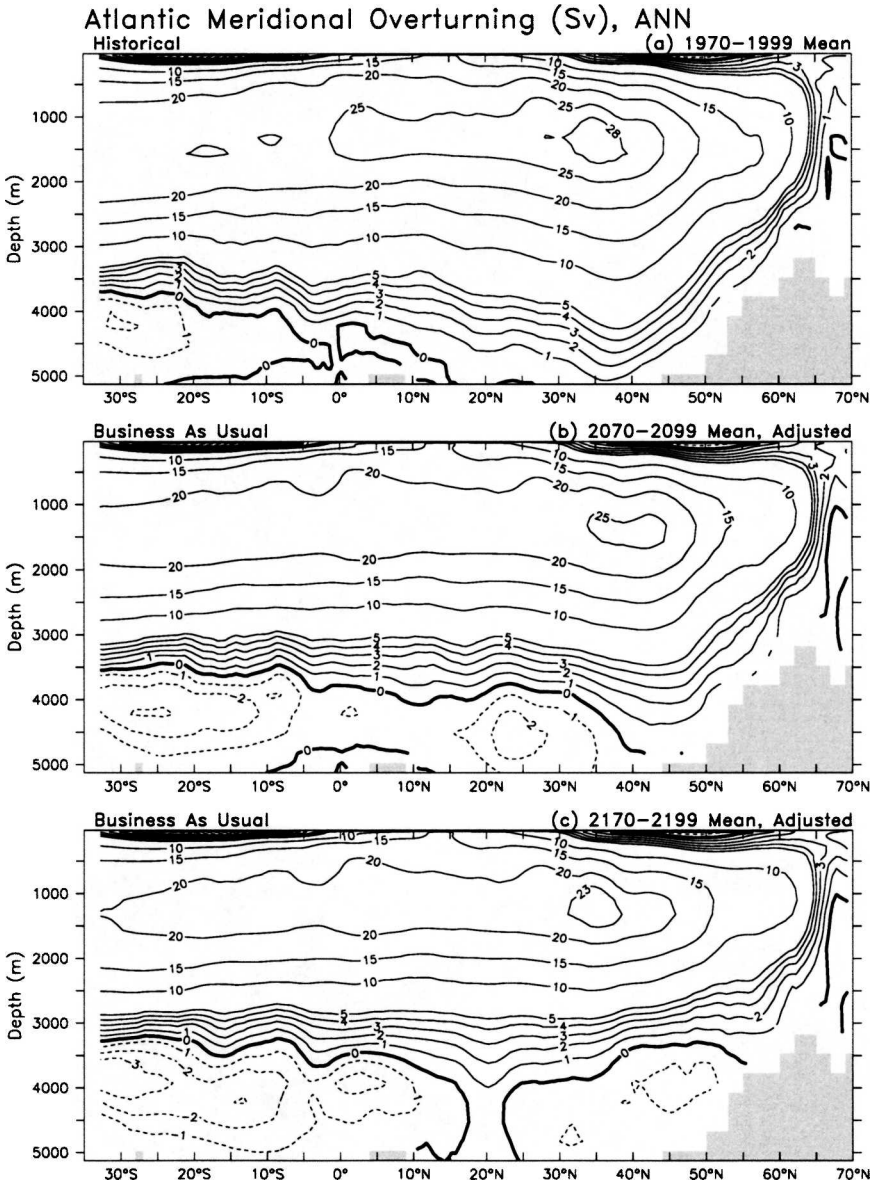

FIG. 16. Zonally averaged annual meridional overturning streamfunction (Sv) for the Atlantic Ocean for period (a) 1970–99 from the historical run, and (b) 2070–99 and (c) 2170–99 under the BAU scenario. The unforced drifts in this streamfunction during the corresponding period of the control run were removed in this plot.

multidecadal THC variability is mainly driven by the low-frequency atmospheric flux forcing, especially that associated with the NAO. Our results show that the THC-associated variations in SST and sea ice over the North Atlantic in the PCM resemble observed SST and sea ice patterns that are associated with the NAO. The results show that the variations in the SST, sea ice, and other surface fields are probably caused by the THC oscillation as the THC leads the surface fields by 2–3 yr. In other words, in the PCM the NAO is likely affected by the THC oscillation through the influence of the THC-induced SST changes, as suggested by the peak power of NAO variability near the 24-yr time scale (Fig. 6b). However, it is still possible that the near–white noise flux forcing associated with the NAO provides an energy source for the multidecadal THC oscillations.

In the PCM, the 24-yr time scale is determined by the phase lag of ~6 yr between the midlatitude North Atlantic surface ocean density and the THC strength (Fig.

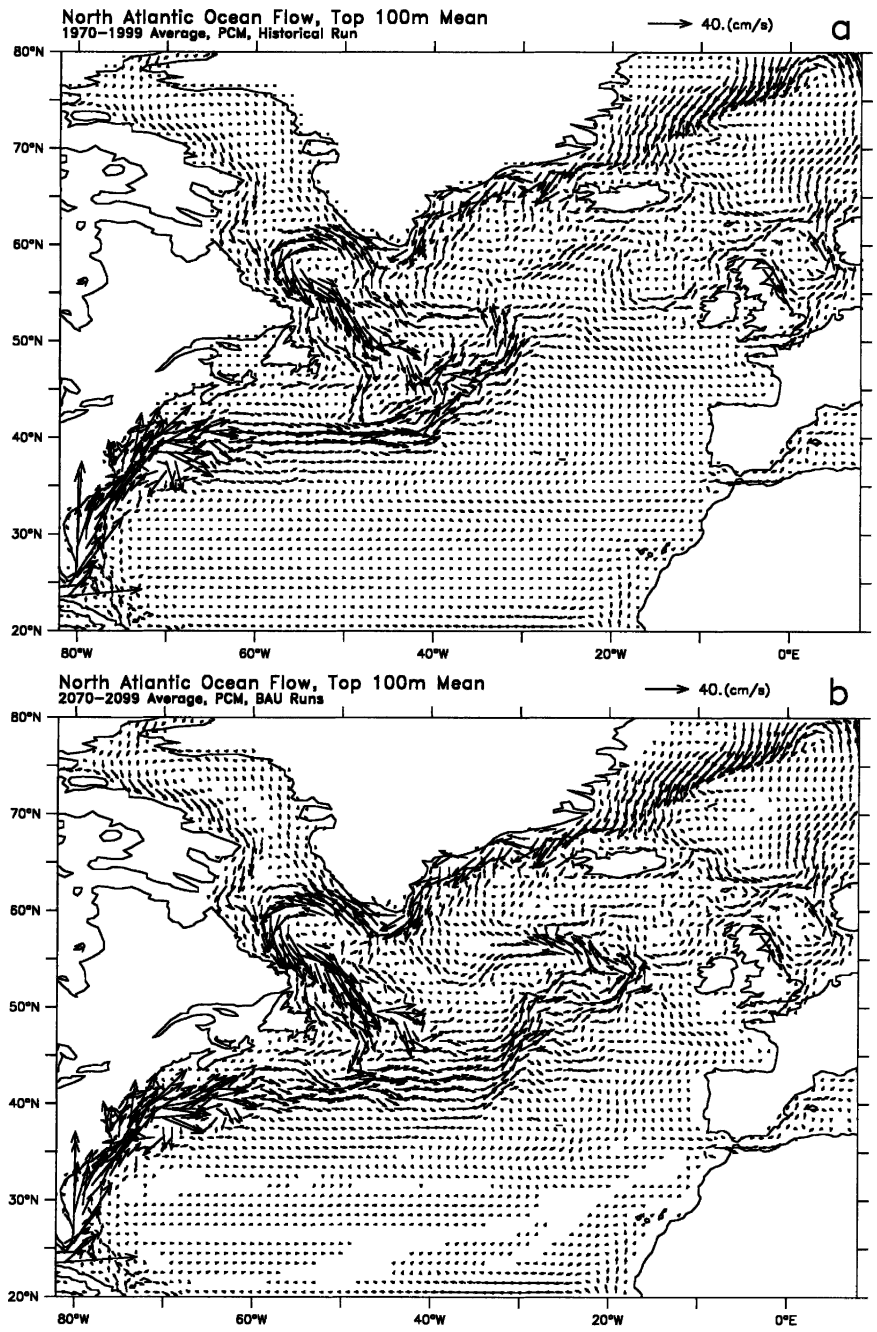

FIG. 17. Top 100-m-averaged annual-mean ocean currents in the North Atlantic for (a) 1970–99 and (b) 2070–99 under the BAU scenario. Current patterns are similar within the top 1.5 km.

10), and this 6-yr lag results from the differential effects of the THC-induced SST and SSS changes on the density (Fig. 9b). The THC affects the SST and SSS mainly through advection (i.e., changes in upper-ocean currents), with secondary feedback effects through changes in lower-tropospheric conditions (stability, cloudiness, precipitation, etc.). It is, however, unclear how the 2–3 yr lags between the variations in the SST, SSS, and other surface fields and the THC oscillations (Fig. 9a) are produced in the model. These time lags appear to be crucial in determining the phase lag between the density and THC and thus the oscillation

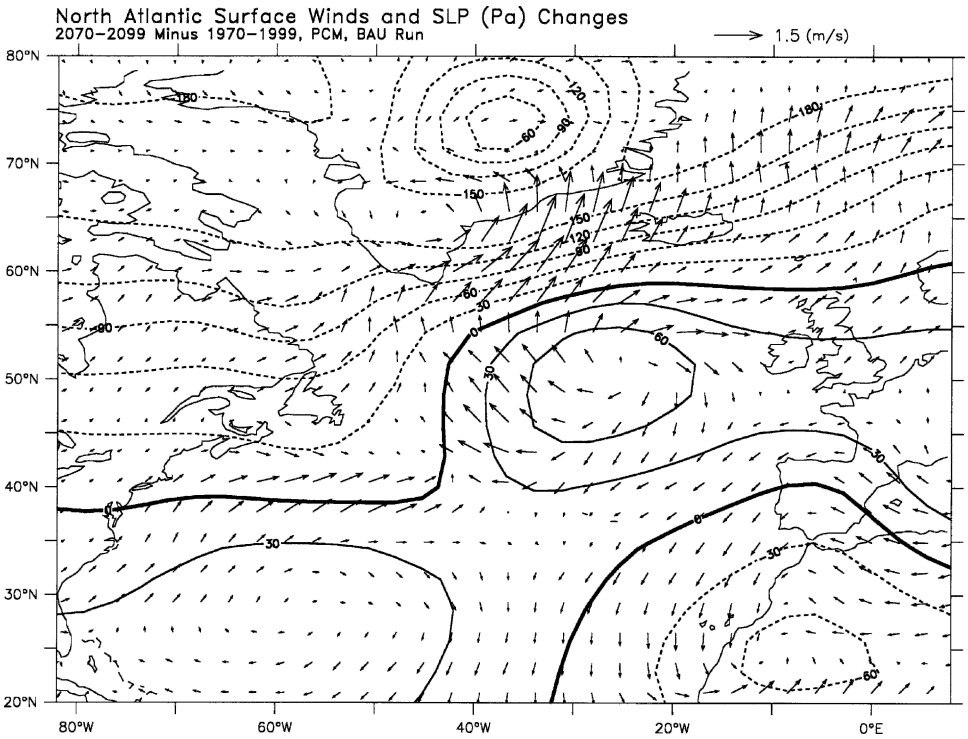

FIG. 18. Changes in annual surface winds (arrows) and mean sea level pressure (contours, interval = 30 Pa, dashed are negative) from 1970–99 to 2070–99 under the BAU scenario. Change patterns for surface wind stress differ only slightly from the wind change patterns.

time scale, although the fact that the SST and SSS variations are slightly different in phase and their effects on density are opposite in sign (Fig. 9b) is very important in producing the density oscillation. Presumably, the upper-ocean advection speed (as shown by Saravanan and McWilliams 1998) and the air–sea heat and freshwater flux exchanges along the path from the subtropics to the mid and high-latitude North Atlantic are major factors influencing the time lags. This suggests that models need to realistically simulate Atlantic Ocean currents in order to produce the correct time scales of multidecadal THC oscillations.

As in observations (Deser et al. 2000), in the PCM the sea ice variations (Fig. 7f) are mostly local thermodynamical response to changes in the SST and surface air temperatures. Most of the NAO-associated wind changes are random (i.e., white noise) and thus cannot be easily linked to the THC oscillation using the PCM simulations. Other model experiments (e.g., Saenko et al. 2003) show large influences of Arctic sea ice on the THC. Furthermore, Holland et al. (2001) show that random wind forcing can still generate multidecadal (~20 yr) variations in the THC through variations in the export of Artic sea ice into the North Atlantic Ocean. Our analyses suggest that the THC multidecadal oscillation results mainly through the advective mechanism (see the introduction) that is associated with large-scale air–sea interactions in the North Atlantic region.

The MOC and the associated NADW and AABW changes that occurred during the 1200-yr control run (Figs. 1 and 4) resemble a seesawing pattern of production of these deep waters between the northern and southern Atlantic Ocean that might have occurred in the real world during the last 1500 yr (Broecker et al. 1999). Chemical and physical oceanographic evidence suggests that less than 5 Sv of the AABW is currently being produced, whereas this number is likely to be around 15 Sv for the past 800 yr (e.g., Broecker et al. 1999). Our model results suggest that such seesawing changes in the MOC and deep-water production are plausible in a fully coupled climate system as the atmosphere and oceans adjust to be consistent with each other. In the real world, any significant disturbance in the atmosphere (such as changes in greenhouse gases) or the oceans (such as sea level changes) might trigger such adjustments and result in the seesawing change of NADW and AABW production. Our CO_2-forced simu-

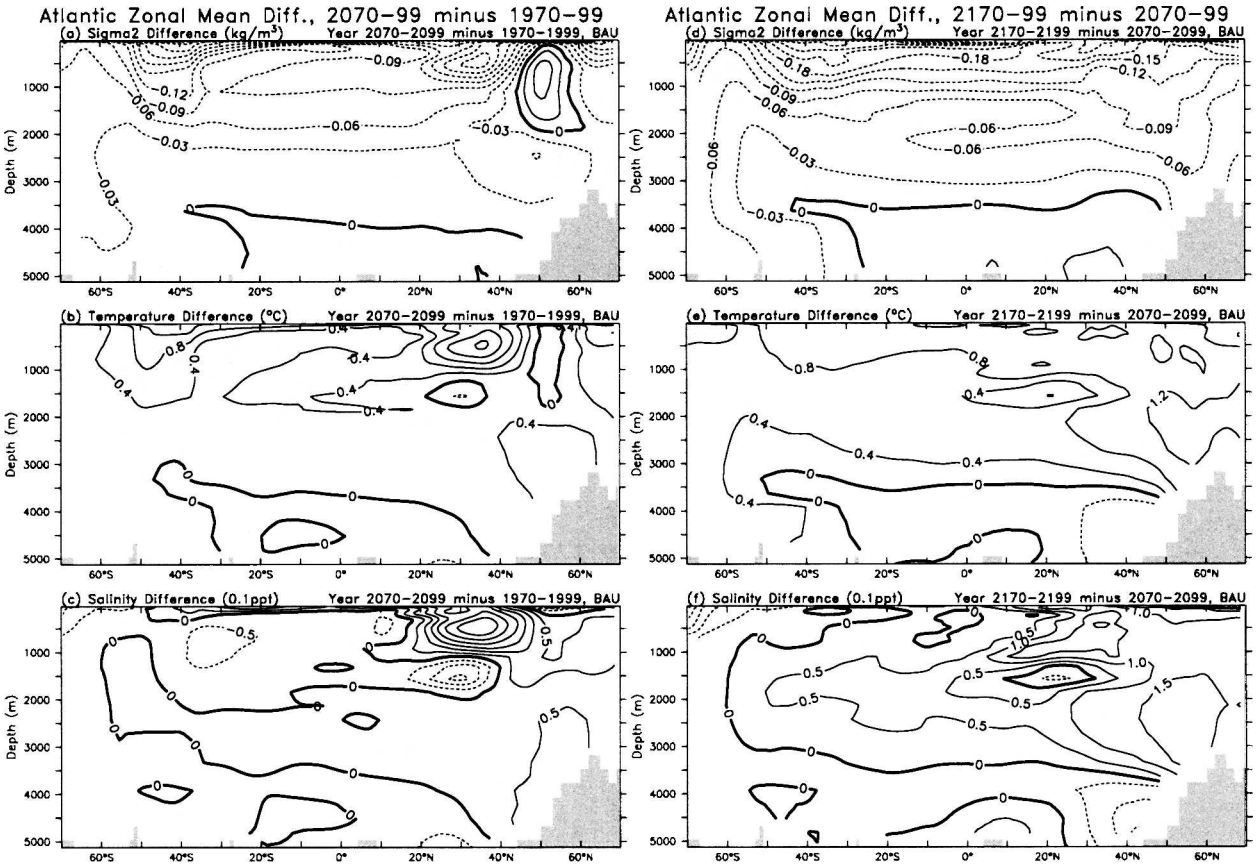

FIG. 19. (left) Atlantic zonal mean difference of year 2070–99 (BAU run) minus 1970–99 for (a) density (kg m^{-3}), (b) temperature (°C), and (c) salinity (0.1 ppt). (right) Same as (left) but for year 2170–99 minus 2070–99 in the BAU case. Dashed lines are for negative values.

lations, however, suggest that a weaker production of the AABW is associated with a stronger THC as the bottom cell of the MOC weakens (Fig. 4). This seems to suggest that the increased greenhouse gas forcing during the last several decades might not have been the cause for the current reduction in the AABW, as the model suggests that the greenhouse gas forcing would weaken the THC and enhance the bottom cell (Fig. 16).

Our results (Figs. 1–3) support the conventional notion that the Atlantic Ocean transports a large amount of heat from the low latitudes into the mid- and high latitudes, which contributes to the relatively warm climate over Europe. The results contradict with Seager et al. (2002) who suggest that a dynamic ocean is not needed and the atmospheric heat transport alone can result in mild winters over Europe. In a fully coupled system like the PCM, the atmospheric and oceanic heat transports in the North Atlantic domain are coupled (e.g., through the coupling of the THC and NAO) and interdependent, with the THC playing an important role.

Currently there is a debate about the role of Southern Ocean processes in driving the MOC in the North Atlantic Ocean (e.g., Toggweiler and Samuels 1998; Gnanadesikan 1999; Levermann and Griesel 2004). The PCM results seem to suggest that both the vertical (upper versus deep) and meridional (north versus south) gradients of ocean density are important for the THC, which implies that both vertical mixing and Southern Ocean processes can affect the MOC. In the transient experiments with increasing CO_2, changes in these gradients both favor a weakened THC.

7. Summary

We have analyzed a 1200-yr unforced control run and climate change simulations under projected greenhouse gas forcing during the next two centuries for changes in Atlantic Ocean circulations as simulated by the PCM, a coupled climate system model that does not use surface flux adjustments. The PCM has relatively high resolution (~2.8° for the atmosphere and 2/3° for the oceans)

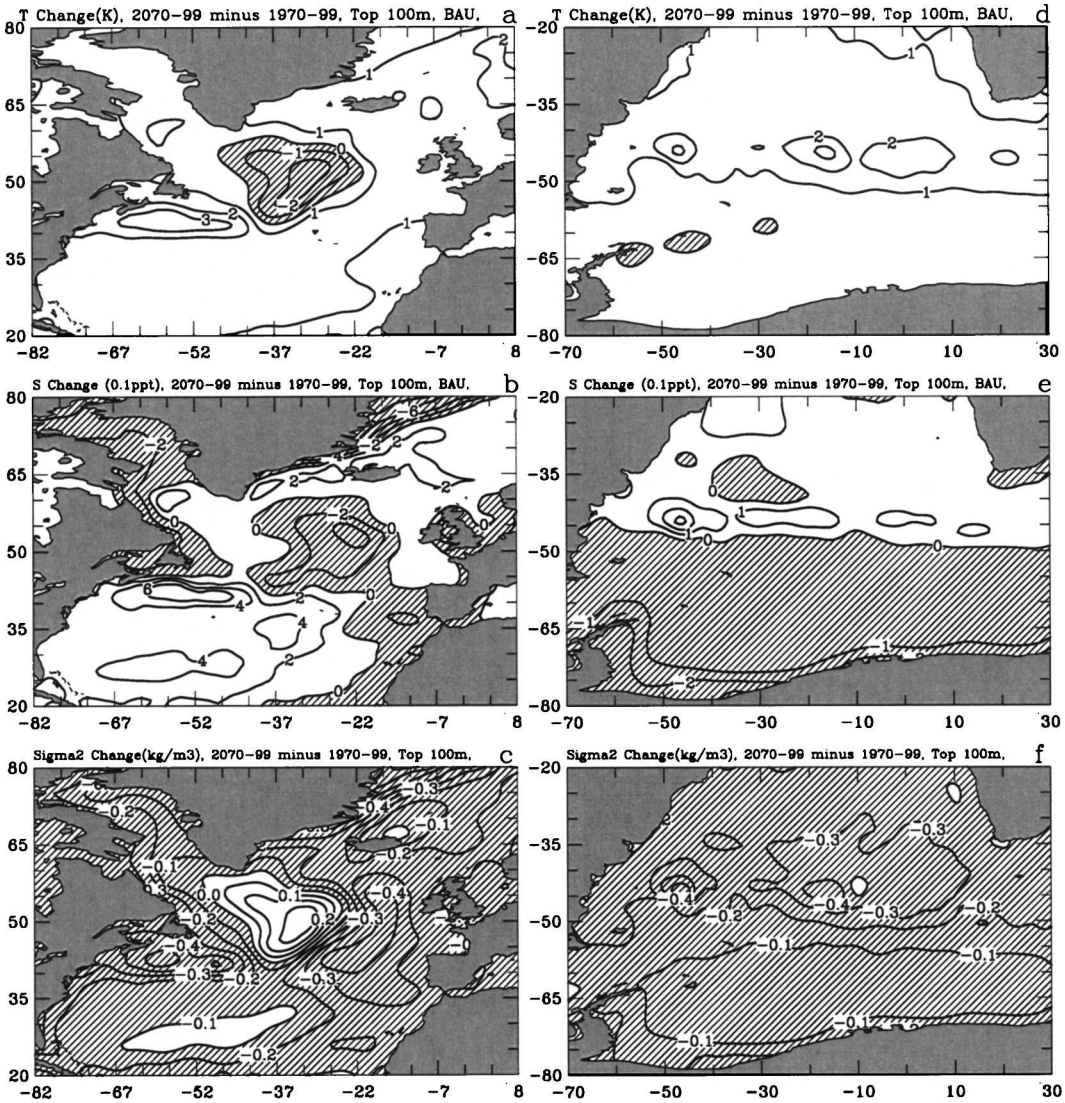

FIG. 20. (left) Changes in top 100-m-averaged ocean (a) temperature (K), (b) salinity (0.1 ppt), and (c) potential density σ_2 in the North Atlantic Ocean from 1970–99 of the historical runs to 2070–99 of the BAU runs. (right) Same as (left) but for the Southern Atlantic Ocean.

and fairly realistic ocean circulations compared with other coupled GCMs. On the other hand, the PCM also has deficiencies, including a stronger than observed THC. Nevertheless, we believe that many of the model results reported here are robust and could have important implications for the Atlantic Ocean circulations, in particular for the THC and its potential response to projected future greenhouse gas forcing. Our main findings are summarized as follows.

The strength of the Atlantic THC shows large variability with (mean peak) amplitudes of 1.5–3.0 Sv around 15–40-yr time scales, with a sharp peak of power around 24 yr in the 1200-yr control run. During periods of strong THC, more heat is transported from low latitudes and converged into the northern midlatitude Atlantic Ocean, resulting in above-normal SST and surface air temperature over midlatitude Atlantic (0.3°–0.6°C warmer) and Eurasia (0.2°–0.4°C) (cf. Fig. 3). This is in contrast to Seager et al. (2002) who claim that atmospheric heat transport alone is responsible for mild winters over Europe. Associated with the THC multidecadal oscillation, there are large variations in North Atlantic SST, SSS, sea ice fraction, and net surface water and energy fluxes, which all lag the THC by 2–3 yr. However, the net effect of the SST and SSS variations on upper-ocean density in the midlatitude North At-

lantic leads the THC by ~6 yr or 90° in phase (Fig. 10). This phase shift provides the direct mechanism for the 24-yr THC cycle to oscillate through density's effect on NADW formation.

Comparisons with observed SST (1900–2003) and sea ice concentration (1953–2003) show that the SST and sea ice modes associated with the THC oscillation in the PCM resemble the spatial patterns of the observed SST and sea ice variations that are associated with the NAO, although the time scales with peak power in the relatively short records of SST and NAO index are considerably shorter, around 13 and 8 yr, respectively. Another finding is that the leading EOF of the observed North Atlantic (20°–70°N) SST shows large warming around 30°–55°N whose temporal evolution closely follows Northern Hemispheric ($r = 0.79$) and global ($r = 0.72$) mean surface temperatures since 1900.

The results suggest that the THC multidecadal oscillation in the PCM is coupled with the NAO, whose index also shows the largest peak of power around 24 yr that is nearly in phase with the THC in the model. With the THC leading the SST, the NAO's variability around the 24-yr time scale is probably induced by the THC. On the other hand, it is still possible that the near–white noise flux forcing associated with the NAO provides an energy source for the THC oscillations.

Forced by projected CO_2 and other trace gases for the next two centuries, the PCM shows significant weakening (by ~12%) of the THC during the twenty-first century, even after removing the unforced THC drift during the period. In the twenty-second century, the THC continues to weaken (by an additional ~10%) if atmospheric CO_2 keeps rising, but stabilizes if the CO_2 levels off.

In the forced simulations, the upper Atlantic Ocean warms faster than the deeper ocean, which results in larger density decreases in the upper ocean than below. Furthermore, the warming is larger in the North Atlantic sinking region (north of 45°N) than in the southern end of the basin (south of 55°S), which results in larger density decreases in the northern North Atlantic than in the Southern Ocean. These differential density changes weaken the THC and enhance the bottom cell of the Atlantic MOC (i.e., the AABW). Salinity changes in the Atlantic Ocean (Fig. 19) are relatively small in the forced simulations, as net surface water flux changes little.

Accompanying the THC changes, the position of the separated GS, the subpolar gyre centered at the Labrador Sea, and the NAC path also change in both the control and forced runs. Specifically, as the THC gains (loses) strength and depth, the separated GS moves southward (northward), while the subpolar gyre contracts from (expands to) the east with the NAC path being shifted westward (eastward). These horizontal circulation changes are dynamically linked to the THC changes through the bottom vortex stretching induced by a downslope DWBC (ZV).

The THC and the associated horizontal current changes have large effects on ocean temperature and salinity in the North Atlantic Ocean. Specifically, when the THC is strong and the subpolar gyre contracts from the east while the separated GS shifts southward, the water south of the Greenland tip becomes warmer and saltier while the region around the mean GS path (39°–44°N, 40°–67°W) becomes colder and fresher.

Our results confirm previous findings (e.g., Delworth et al. 1993; Delworth and Greatbatch 2000; Cheng et al. 2004) that the Atlantic THC and the associated deep-water production may have self-regulating mechanisms that allows them to oscillate from one strong state to another weak state or vice versa on multidecadal time scales. Our analyses suggest a dominant role of the advective mechanism, with strong air–sea coupling, in producing the THC multidecadal oscillations. The results also show that the THC weakens whenever ocean density decreases more in the upper or the northern end of the Atlantic Ocean than in the deeper or southern end of the Atlantic Ocean, or vice versa. Because the greenhouse gas–induced warming should gradually penetrate into the deep oceans and the warming should be larger in the Northern Hemisphere (due to more landmass) than in the Southern Hemisphere, the thermal effect of the warming should weaken the THC, although changes in freshwater fluxes may have larger effects in other models than in the PCM. The latter could be the main reason for different THC responses to increased greenhouse gas forcing among some of the coupled models.

Acknowledgments. We thank Ron Stouffer and another anonymous reviewer for helpful comments; Clara Deser, Frank Bryan, Young-oh Kwon, and Rong Zhang for constructive discussions; and Adam Phillips for assistance with the HadISST dataset, which was provided by the Met Office Hadley Centre for Climate Prediction and Research. T.W. Bettge, J.M. Arblaster, J.W. Weatherly, V.B. Wayland, and A.P. Craig contributed to the PCM simulations, which were supported by the Office of Biological and Environmental Research, U.S. Department of Energy, and U.S. National Science Foundation.

REFERENCES

Ammann, C. M., G. A. Meehl, W. M. Washington, and C. S. Zender, 2003: A monthly and latitudinally varying volcanic forc-

ing dataset in simulations of the 20th century climate. *Geophys. Res. Lett.,* **30,** 1657, doi:10.1029/2003GL016875.

Belkin, I. M., S. Levitus, J. Antonov, and S.-A. Malmberg, 1998: "Great salinity anomalies" in the North Atlantic. *Progress in Oceanography,* Vol. 41, Pergamon, 1–68.

Boer, G. J., G. Flato, and D. Ramsden, 2000: A transient climate change simulation with greenhouse gas and aerosol forcing: Projected climate for the 21st century. *Climate Dyn.,* **16,** 427–450.

Boville, B. A., and P. R. Gent, 1998: The NCAR Climate System Model, version one. *J. Climate,* **11,** 1115–1130.

Broecker, W. S., 1987: Unpleasant surprises in the greenhouse? *Nature,* **328,** 123–126.

——, 1997: Thermohaline circulation, the Achilles heel of our climate system: Will man-made CO_2 upset the current balance? *Science,* **278,** 1582–1588.

——, S. Sutherland, and T.-H. Peng, 1999: A possible 20th-century slowdown of Southern Ocean deep water formation. *Science,* **286,** 1132–1135.

Bryan, F. O., 1986: High-latitude salinity effects and interhemispheric thermohaline circulations. *Nature,* **323,** 301–304.

Bryan, K., 1984: Accelerating the convergency to equilibrium of ocean-climate models. *J. Phys. Oceanogr.,* **14,** 666–673.

Bryden, H. L., and S. Imawaki, 2001: Ocean heat transport. *Ocean Circulation and Climate*, S. Siedler, J. Church, and J. Gould, Eds., Academic Press, 455–474.

Cheng, W., R. Bleck, and C. Rooth, 2004: Multi-decadal thermohaline variability in an ocean–atmosphere general circulation model. *Climate Dyn.,* **22,** 573–590.

Clark, P. U., N. G. Pisias, T. F. Stocker, and A. J. Weaver, 2002: The role of the thermohaline circulation in abrupt climate change. *Nature,* **415,** 863–869.

Cubasch, U., and Coauthors, 2001: Projections of future climate change. *Climate Change 2001: The Scientific Basis*, J. T. Houghton et al., Eds., Cambridge University Press, 525–582.

Curry, R., B. Dickson, and I. Yashayaev, 2003: A change in the freshwater balance of the Atlantic Ocean over the past four decades. *Nature,* **426,** 826–829.

Dai, A., G. A. Meehl, W. M. Washington, T. M. L. Wigley, and J. M. Arblaster, 2001a: Ensemble simulation of twenty-first century climate changes: Business-as-usual versus CO_2 stabilization. *Bull. Amer. Meteor. Soc.,* **82,** 2377–2388.

——, ——, ——, and ——, 2001b: Climate changes in the twenty-first century over the Asia-Pacific region simulated by the NCAR CSM and PCM. *Adv. Atmos. Sci.,* **18,** 639–658.

——, T. M. L. Wigley, G. A. Meehl, and W. M. Washington, 2001c: Effects of stabilizing atmospheric CO_2 on global climate in the next two centuries. *Geophys. Res. Lett.,* **28,** 4511–4514.

——, ——, B. A. Boville, J. T. Kiehl, and L. E. Buja, 2001d: Climates of the twentieth and twenty-first centuries simulated by the NCAR Climate System Model. *J. Climate,* **14,** 485–519.

——, W. M. Washington, G. A. Meehl, T. W. Bettge, and W. G. Strand, 2004: The ACPI climate change simulations. *Climate Change,* **62,** 29–43.

Danabasoglu, G., J. C. McWilliams, and W. G. Large, 1996: Approach to equilibrium in accelerated global oceanic models. *J. Climate,* **9,** 1092–1110.

Delworth, T. L., and R. J. Greatbatch, 2000: Multidecadal thermohaline circulation variability driven by atmospheric surface flux forcing. *J. Climate,* **13,** 1481–1495.

——, S. Manabe, and R. J. Stouffer, 1993: Interdecadal variations of the thermohaline circulation in a coupled ocean–atmosphere model. *J. Climate,* **6,** 1993–2011.

Deser, C., and M. L. Blackmon, 1993: Surface climate variations over the North-Atlantic Ocean during winter: 1900–1989. *J. Climate,* **6,** 1743–1753.

——, J. E. Walsh, and M. S. Timlin, 2000: Arctic sea ice variability in the context of recent atmospheric circulation trends. *J. Climate,* **13,** 617–633.

——, M. Holland, G. Reverdin, and M. Timlin, 2002: Decadal variations in Labrador Sea ice cover and North Atlantic sea surface temperatures. *J. Geophys. Res.,* **107,** 3035, doi:10.1029/2000JC000683.

Dickson, B., I. Yashayaev, J. Meincke, B. Turrell, S. Dye, and J. Holfort, 2002: Rapid freshening of the deep North Atlantic Ocean over the past four decades. *Nature,* **416,** 832–837.

Dickson, R., J. Lazier, J. Meincke, P. Rhines, and J. Swift, 1996: Long-term cooridinated changes in the convective activity of the North Atlantic. *Progress in Oceanography,* Vol. 38, Pergamon, 241–295.

Dixon, K. W., T. L. Delworth, M. J. Spelman, and R. J. Stouffer, 1999: The influence of transient surface fluxes on North Atlantic overturning in a coupled GCM climate change experiment. *Geophys. Res. Lett.,* **26,** 2749–2752.

——, ——, T. R. Knutson, M. J. Spelman, and R. J. Stouffer, 2003: A comparison of climate change simulations produced by two GFDL coupled climate models. *Global Planet. Change,* **37,** 81–102.

Dukowicz, J. K., and R. D. Smith, 1994: Implicit free-surface method for Bryan-Cox-Semtner ocean model. *J. Geophys. Res.,* **99,** 7991–8014.

Gent, P. R., 2001: Will the North Atlantic Ocean thermohaline circulation weaken during the 21st century? *Geophys. Res. Lett.,* **28,** 1023–1026.

Gnanadesikan, A., 1999: A simple predictive model for the structure of the oceanic pycnocline. *Science,* **283,** 2077–2079.

Griffies, S. M., and K. Bryan, 1997: Predictability of North Atlantic multidecadal climate variability. *Science,* **275,** 181–184.

Häkkinen, S., and P. B. Rhines, 2004: Decline of subpolar North Atlantic circulation during the 1990s. *Science,* **304,** 555–559.

Hansen, B., W. R. Turrell, and S. Osterhus, 2001: Decreasing overflow from the Nordic seas into the Atlantic Ocean through the Faroe Bank channel since 1950. *Nature,* **411,** 927–930.

Holland, M. M., C. M. Bitz, M. Eby, and A. J. Weaver, 2001: The role of ice–ocean interactions in the variability of the North Atlantic thermohaline circulation. *J. Climate,* **14,** 656–675.

Hu, A., G. A. Meehl, W. M. Washington, and A. Dai, 2004: Response of the Atlantic thermohaline circulation to increased atmospheric CO_2 in a coupled model. *J. Climate,* **17,** 4267–4279.

Hughes, T. M. C., and A. J. Weaver, 1996: Sea surface temperature–evaporation feedback and the ocean's thermohaline circulation. *J. Phys. Oceanogr.,* **26,** 644–654.

Hurrell, J. W., 1995: Decadal trends in the North Atlantic Oscillation—Regional temperatures and precipitation. *Science,* **269,** 676–679.

Jones, P. D., and A. Moberg, 2003: Hemispheric and large-scale surface air temperature variations: An extensive revision and an update to 2001. *J. Climate,* **16,** 206–223.

Joyce, T. M., C. Deser, and M. A. Spall, 2000: The relation between decadal variability of subtropical mode water and the North Atlantic Oscillation. *J. Climate,* **13,** 2550–2569.

Knight, J. R., R. J. Allan, C. K. Folland, and M. Vellinga, 2003:

Quasi-periodic natural variations in the thermohaline circulation and climate in a 1400 year coupled model calculation. Preprints, *14th Symp. on Global Change and Climate Variations*, Long Beach, CA, Amer. Meteor. Soc., CD-ROM, P13.11.

Kushnir, Y., 1994: Interdecadal variations in North Atlantic sea surface temperature and associated atmospheric conditions. *J. Climate,* **7,** 141–157.

Latif, M., E. Roeckner, U. Milkolajewicz, and R. Voss, 2000: Tropical stabilization of thermohaline circulation in a greenhouse warming simulation. *J. Climate,* **13,** 1809–1813.

Lenderink, G., and R. J. Haarsma, 1994: Variability and multiple equilibria of the thermohaline circulation associated with deep-water formation. *J. Phys. Oceanogr.,* **24,** 1480–1493.

Levermann, A., and A. Griesel, 2004: Solution of a model for the oceanic pycnocline depth: Scaling of overturning strength and meridional pressure difference. *Geophys. Res. Lett.,* **31,** L17302, doi:10.1029/2004GL020678.

Levitus, S., and T. Boyer, 1994: *Temperature.* Vol. 4, *World Ocean Atlas 1994,* NOAA Atlas NESDIS 4, 117 pp.

——, R. Burgett, and T. Boyer, 1994: *Salinity*. Vol. 3, *World Ocean Atlas 1994,* NOAA Atlas NESDIS 3, 99 pp.

Manabe, S., and R. J. Stouffer, 1994: Multi-century response of a coupled ocean–atmosphere model to an increase of atmospheric carbon dioxide. *J. Climate,* **7,** 5–23.

——, and ——, 1997: Coupled ocean-atmosphere model response to freshwater input: Comparison to the Younger Dryas event. *Paleoceanography,* **12,** 321–336.

Marotzke, J., and J. Willebrand, 1991: Multiple equilibria of the global thermohaline circulation. *J. Phys. Oceanogr.,* **21,** 1372–1385.

Marsh, R., 2000: Recent variability of the North Atlantic thermohaline circulation inferred from surface heat and freshwater fluxes. *J. Climate,* **13,** 3239–3260.

Meehl, G. A., P. R. Gent, J. M. Arblaster, B. Otto-Bliesner, E. C. Brady, and A. P. Craig, 2001: Factors that affect amplitude of El Niño in global coupled climate models. *Climate Dyn.,* **17,** 515–526.

——, W. M. Washington, T. M. L. Wigley, J. M. Arblaster, and A. Dai, 2003: Solar and greenhouse gas forcing and climate response in the twentieth century. *J. Climate,* **16,** 426–444.

Mikolajewicz, U., and E. Maier-Reimer, 1994: Mixed boundary conditions in ocean general circulation models and their influence on the stability of the model's conveyor belt. *J. Geophys. Res.,* **99,** 22 633–22 644.

——, and R. Voss, 2000: The role of the individual air-sea flux components in CO_2-induced changes of the ocean's circulation and climate. *Climate Dyn.,* **16,** 627–642.

Nakićenović, N., and R. Swart, Eds., 2000: *IPCC Special Report on Emission Scenarios*. Cambridge University Press, 570 pp.

Rahmstorf, S., 1995: Bifurcations of the Atlantic thermohaline circulation in response to changes in the hydrological cycle. *Nature,* **378,** 145–149.

——, 1999: Shifting seas in the greenhouse? *Nature,* **399,** 523–524.

——, 2002: Ocean circulation and climate during the past 120 000 years. *Nature,* **419,** 207–214.

——, and A. Ganopolski, 1999: Long-term global warming scenarios computed with an efficient coupled climate model. *Climate Change,* **43,** 353–367.

——, J. Marotzke, and J. Willebrand, 1996: Stability of the thermohaline circulation. *The Warm Watersphere of the North Atlantic Ocean*, W. E. Krauss, Ed., Bornträger, 129–157.

Rayner, N. A., D. E. Parker, E. B. Horton, C. K. Folland, L. V. Alexander, D. P. Rowell, E. C. Kent, and A. Kaplan, 2003: Global analyses of sea surface temperature, sea ice, and night marine air temperature since the late nineteenth century. *J. Geophys. Res.,* **108,** 4407, doi:10.1029/2002JD002670.

Russell, G. L., and D. Rind, 1999: Response to CO_2 transient increase in the GISS coupled model: Regional coolings in a warming climate. *J. Climate,* **12,** 531–539.

Saenko, O. A., E. C. Wiebe, and A. J. Weaver, 2003: North Atlantic response to the above-normal export of sea ice from the Arctic. *J. Geophys. Res.,* **108,** 3224, doi:10.1029/2001JC001166.

Saravanan, R., and J. C. McWilliams, 1998: Advective ocean–atmosphere interaction: An analytical stochastic model with implications for decadal variability. *J. Climate,* **11,** 165–188.

——, G. Danabasoglu, S. C. Doney, and J. C. McWilliams, 2000: Decadal variability and predictability in the midlatitude ocean–atmosphere system. *J. Climate,* **13,** 1073–1097.

Schmittner, A., and T. F. Stocker, 1999: The stability of the thermohaline circulation in global warming experiments. *J. Climate,* **12,** 1117–1133.

Seager, R., D. S. Battisti, J. Yin, N. Gordon, N. Naik, A. C. Clement, and M. A. Cane, 2002: Is the Gulf Stream responsible for Europe's mild winters? *Quart. J. Roy. Meteor. Soc.,* **128,** 2563–2586.

Smith, R. D., J. K. Dukowicz, and R. C. Malone, 1992: Parallel ocean general circulation modeling. *Physica D,* **60,** 38–61.

Stocker, T. F., 2000: Past and future reorganizations in the climate system. *Quat. Sci. Rev.,* **19,** 301–319.

——, and D. G. Wright, 1991: Rapid transitions of the ocean's deep circulation induced by changes in surface water fluxes. *Nature,* **351,** 729–732.

——, and A. Schmittner, 1997: Influence of CO_2 emission rates on the stability of the thermohaline circulation. *Nature,* **388,** 862–865.

Stommel, H., 1961: Thermohaline convection with two stable regimes of flow. *Tellus,* **13,** 224–230.

Stouffer, R. J., and S. Manabe, 2003: Equilibrium response of thermohaline circulation to large changes in atmospheric CO_2 concentration. *Climate Dyn.,* **20,** 759–773.

Sun, S., and R. Bleck, 2001: Atlantic thermohaline circulation and its response to increasing CO_2 in a coupled atmosphere-ocean model. *Geophys. Res. Lett.,* **28,** 4223–4226.

Thorpe, R. B., J. M. Gregory, T. C. Johns, R. A. Wood, and J. F. B. Mitchell, 2001: Mechanisms determining the Atlantic thermohaline circulation response to greenhouse gas forcing in a non-flux-adjusted coupled climate model. *J. Climate,* **14,** 3102–3116.

Toggweiler, J. R., and B. Samuels, 1998: On the ocean's large-scale circulation near the limit of no vertical mixing. *J. Phys. Oceanogr.,* **28,** 1832–1852.

Trenberth, K. E., and J. M. Caron, 2001: Estimates of meridional atmosphere and ocean heat transport. *J. Climate,* **14,** 3433–3443.

Voss, R., and U. Milkolajewicz, 2001: Long-term climate changes due to increased CO_2 concentration in the coupled atmosphere-ocean general circulation model ECHAM3/LSG. *Climate Dyn.,* **17,** 45–60.

Washington, W. M., and Coauthors, 2000: Parallel Climate Model

(PCM) control and transient simulations. *Climate Dyn.,* **16,** 755–774.

Weaver, A. J., and E. S. Sarachik, 1991: Evidence for decadal variability in an ocean general circulation model: An advective mechanism. *Atmos.–Ocean,* **29,** 197–231.

——, and S. Valcke, 1998: On the variability of thermohaline circulation in the GFDL coupled model. *J. Climate,* **11,** 759–767.

——, J. Marotzke, P. F. Cummins, and E. S. Sarachik, 1993: Stability and variability of the thermohaline circulation. *J. Phys. Oceanogr.,* **23,** 39–60.

——, S. M. Aura, and P. G. Myers, 1994: Interdecadal variability in an idealized model of the North Atlantic. *J. Geophys. Res.,* **99,** 12 423–12 441.

Wiebe, E. C., and A. J. Weaver, 1999: On the sensitivity of global warming experiments to the parameterization of sub-grid scale ocean mixing. *Climate Dyn.,* **15,** 875–893.

Winton, M., and E. S. Sarachik, 1993: Thermohaline oscillations induced by strong steady salinity forcing of ocean general circulation models. *J. Phys. Oceanogr.,* **23,** 1389–1410.

Wood, R. A., A. B. Keen, J. F. B. Mitchell, and J. M. Gregory, 1999: Changing spatial structure of the thermohaline circulation in response to atmospheric CO_2 forcing in a climate model. *Nature,* **399,** 572–575.